Tissue libraries enable rapid determination of conditions that preserve antibody labeling in cleared mouse and human tissue

Theodore J. Zwang[1,2,3], Rachel E. Bennett[1,2,3], Maria Lysandrou[1], Benjamin Woost[1], Anqi Zhang[4], Charles M. Lieber[5], Douglas S. Richardson[6], Bradley T. Hyman[1,2,3]

[1]Department of Neurology, Massachusetts General Hospital, Harvard Medical School, Boston, MA, USA
[2]Harvard Medical School, Boston, MA, USA
[3]Massachusetts Alzheimer's Disease Research Center, Charlestown, MA, USA
[4]Department of Chemical Engineering, Stanford University, Stanford, CA, USA
[5]Department of Chemistry and Chemical Biology, Harvard University, Cambridge, MA, USA
[6]Department of Molecular and Cellular Biology and Harvard Center for Biological Imaging, Harvard University, Cambridge, MA, USA

Abstract

Difficulty achieving complete, specific, and homogenous staining is a major bottleneck preventing the widespread use of tissue clearing techniques to image large volumes of human tissue. In this manuscript, we describe a procedure to rapidly design immunostaining protocols for antibody labeling of cleared brain tissue. We prepared libraries of .5-1.0 mm thick tissue sections that are fixed, pre-treated, and cleared via similar, but different procedures to optimize staining conditions for a panel of antibodies. Results from a library of mouse tissue correlate well with results from a similarly prepared library of human brain tissue, suggesting mouse tissue is an adequate substitute for protocol optimization. These data show that procedural differences do not influence every antibody-antigen pair in the same way, and minor changes can have deleterious effects, therefore, optimization should be conducted for each target. The approach outlined here will help guide researchers to successfully label a variety of targets, thus removing a major hurdle to accessing the rich 3D information available in large, cleared human tissue volumes.

Introduction

In recent years, there have been substantial improvements in the techniques used to visualize features of brains, organs, and whole organisms in three dimensions. One promising method, tissue clearing, involves lipid removal and refractive index matching to significantly decrease light scattering. Tissue clearing allows for light microscopy to observe the distribution of individual molecules throughout entire organs millimeters to centimeters in size.[1,2] This holds extraordinary promise for understanding human diseases, where the identification and characterization of abnormal structures is often an early step towards the development of clinical treatments.[3] Difficulties with antibody staining and labeling is common in traditional thin tissue section histology, but is dramatically amplified in large, cleared samples. Although techniques have been developed to improve the homogeneity of staining (SWITCH[4]) and increase the speed of antibody labeling in large, cleared tissue (eFlash[5], EFIC[6], MDH[7]), these methods only work if an antibody's epitope is well preserved during the tissue preparation and clearing process. This is rarely the case and complete, specific and homogenous staining is now the most common bottleneck preventing the widespread use of tissue clearing in samples that cannot be modified to express fluorescent proteins such as human tissue. Therefore, most tissue clearing methods

have been optimized for studies in rodents, and only a few recent studies apply clearing techniques to human tissue.[8-12] Here, we present a simple optimization strategy and automated analysis routine that allows researchers to tune their immunohistochemistry protocols for labeling protein targets in cleared and uncleared brain tissue. Further, we demonstrate that our optimized protocols can be extended from mouse to human tissue.

Immunohistochemistry (IHC) has a history of being difficult, with myriad improvements taking place over decades to allow for its current ubiquity in pathology laboratories and biomarker discovery.[11] The basic concept of IHC is to use antibodies to label specific antigens in a sample, which can then be imaged to determine the antigen's distribution. Successful IHC requires four fundamentals: 1) the antibody cannot denature, 2) the epitope cannot denature, 3) the antibody must diffuse completely through the tissue and 4) the antibody must only bind its intended target. Often researchers develop lengthy protocols that include steps thought to enable successful labeling but are not necessarily based on empirical evidence or are borrowed from others using completely different antibodies or tissues. In general, IHC protocols share several common steps: first components of the tissue must be fixed in place to preserve its structure. This is typically performed by freezing the tissue or placing it in an aldehyde containing solution like formalin. It may then be stored for long periods of time before an investigation is initiated. Next, different methods of antigen retrieval can be deployed to enhance antibody binding. The tissue may also be blocked by incubating with serum or other agents to deactivate endogenous enzymes and reduce non-specific antibody staining. Finally, when labeling and imaging thick tissue, tissue clearing protocols are required that introduce several additional chemical treatments including dehydration, hydrogel embedding, delipidation, and immersion in a solution that is refractive index matched to the processed tissue[2,13].

It is well understood that differences in staining quality can result from biological heterogeneity such sa small differences in tissue composition, individual antibodies, their epitopes, and overall tissue structure. However, further variability can be induced by each step of an IHC protocol[3,11,14]. Because of this, IHC protocols can usually be reproduced with the same tissues, antibodies, and fluorophores. Unfortunately, it is common to have difficulties extending these protocols to different antibodies or tissues. The complexity of these multi-step protocols makes it prohibitively costly and time-intensive for researchers to optimize all possible IHC conditions for their specific study. This has slowed the testing and adoption of reported improvements in IHC procedures as many researchers are forced to guess at the best protocol for their samples.

Experiments with human tissue samples are essential for a complete understanding of the pathology of many diseases. However, the necessary optimization of IHC protocols described above is often not possible in human tissue due to its scarcity. Attempting to use IHC protocols optimized for different tissues or antibodies could confound results and limit the insight gained from such precious resources. Ideally, researchers could optimize protocols in a more plentiful model species such as mice and directly transfer these methods to human samples. However, it is not often clear whether IHC improvements in mice[4,15,16] would translate to better staining of human tissue. Methods that can rapidly determine optimal IHC protocols for individual antibodies and assess their applicability to tissues from different species are needed.

Inspired by our previous experience troubleshooting IHC in large volumes of mouse brain tissue, we developed a practical workflow to rapidly optimize IHC protocols for different antibodies. We then

applied this methodology to a variety of targets in mouse and human brain tissue to understand 1) how much variation exists if IHC protocols are optimized for individual antibodies and 2) if optimized IHC protocols can be generalized between species. We compare the effect of different IHC protocols on antibodies and a small molecule DNA label, 4',6-diamidino-2-phenylindole (DAPI). We also test the influence of protocols on different antibodies raised against the same protein target and finally, explore whether IHC protocols optimized in mouse tissue can produce equally high-quality staining in human tissue. Together this work provides a method to empirically determine the optimal procedure for IHC studies in large volume tissue, assess its generalizability, and supports the use of abundant mouse tissue to optimize IHC protocols for scarce human samples.

Results

Strategy to rapidly assess the optimization of protocols

Our workflow for determining an optimal IHC protocol is inspired by the success of quantitative structure-activity relationship modeling (QSAR) for drug discovery. QSAR models are used to predict the biological activities of untested drugs by first testing a library of drugs with similar but varied structures, measuring how each drug affects the activity, then creating a model that relates the structural changes to the observed activities.[17] Borrowing from this strategy and making a library of tissues that all went through similar processing steps but for a few key changes allows for us to predict the optimal staining protocol without needing to test every possible combination of conditions.

The use of large intact organs such as whole mouse brains is unnecessary and impractical for optimizing an IHC protocol. However, if the tissue sections are too thin, the impact of antibody diffusion cannot be fully appreciated and compared across protocols; whereas, if the sections are too thick, extensive incubation times are required. Through empirical testing, we found tissue sections 0.5-1.0 mm thick and antibody incubation times of 18-24 hours to be sufficient to assess the influence of our chosen conditions on IHC staining quality (Figure S1), and allows dozens of protocols or multiple antibodies to be tested with tissue from a single mouse brain depending on the epitope distribution.

Using QSAR as a guide, we selected 14 conditions to test in our proof-of-principle studies (Scheme 1). These conditions were divided across four standard IHC/tissue clearing steps: fixation, blocking/unmasking, delipidation and antibody incubation. Two conditions were later omitted, and multiple 0.5-1.0 mm thick tissue sections were assigned to 12 protocols to create the final tissue library (Scheme 1). With the library complete, a tissue sections from each condition could be selected for further head-to-head analysis in our image analysis pipeline that outputs a quantifiable metric of quality (see below). Using these metrics, we were able to predict the optimal combination of IHC conditions for each antibody we tested from initial fixation through to final labelling. During this proof-of-principle study, we only tested high quality antibodies that were already known to have high specificity and limited off-target binding for IHC in thin tissue slices.

Measuring IHC quality in cleared tissue

To compare the quality of IHC in the cleared tissue libraries we developed a data analysis pipeline to quickly extract the distribution of fluorescence in multiple samples and derive performance parameters. First, we used one of two different software (Imaris or Ilastik) to generate image segmentation masks. For analysis with Imaris, we isolated objects based on the intensity of fluorescence relative to nearby

background (**Scheme 2**). For analysis with Ilastik, we leveraged machine learning algorithms that allow users to classify pixels and supervise the generation of the segmentation mask[20]. Either of these segmentation masks are then run through code in Matlab that extracts the signal, noise, signal-noise-ratio, area of staining, and the distance into the tissue at which the staining intensity drops by half. IHC quality can then be made by comparing these features across samples.

This analysis does not require staining of images to be perfect nor precise but requires features that can at least be separated via pixel classification. For images with unintended background staining, Ilastik can be trained to separately classify intended and unintended binding. Note that Imaris is also capable of performing similar pixel classification by integrating Labkit, which we did not compare.

After acquiring segmentation results, turning it into an ideal figure of merit will vary depending on the antigen of interest and its distribution in tissue. For antigens that have relatively constant distribution over the depth of imaging, the area of each plane within a z-stack that is segmented could be used as a figure of merit for staining quality across conditions. However, if the antigen distribution does not have a constant distribution, it is better to use a figure of merit that is normalized based on the area of segmentation, such as the average staining intensity at each depth plane.

Conditions that influence antibody and epitope preservation

Starting from a comprehensive collection of published IHC protocols,[2,3,8,13] we selected a subset of commonly varied conditions to create 12 test protocols for proof of principle. Each protocol is nearly identical, only varying by a single condition to allow for a complete understanding of how each change influences staining. The baseline protocol involved minimal processing and gentle conditions. Specifically, the tissue was fixed in 4% paraformaldehyde (PFA) for 2 days post-perfusion, embedded in hydrogel made of 4% acrylamide, delipidated in Sodium dodecyl sulfate (SDS) for 1 day at 37°C, rinsed in phosphate-buffered saline with 0.2% Triton X-100 (PBST) at 4°C, and incubated with antibodies at 4°C for 18 hours. We then created a library of tissue that was processed using small changes to this baseline protocol, so we could compare how each of these changes influenced IHC quality. This library included changes in the composition of the hydrogel (with and without 4% PFA), changes in delipidation time (1 day, 2 days, 3 days), additional steps before antibody incubation (such as unmasking with 50°C or incubation with glycine), and differential changes in antibody incubation temperature (4°C or room temperature). In addition to this library, we also examined the effects of boiling samples in citrate buffer before or after delipidation, heating to temperatures above 70°C before immunolabeling, and removal or decrease of PFA concentration in the transcardial perfusion or post-perfusion fixing step. (**Scheme 1**) However, these conditions were universally observed to negatively impact IHC or tissue integrity, so they were excluded from our final library.

We chose two antibodies commonly used in neuroscience studies of cleared volumes (Glut1 and NeuN) and performed IHC on the same tissue sections from a mouse cortex that were processed according the 12 protocols (**Scheme 1, Figure 1**). Each antibody was directly conjugated to a fluorophore: Glut1 to Alexa Fluor 488 and NeuN to Alexa Fluor 568. Increasing delipidation time to two days had a positive influence on NeuN staining, and no influence on Glut1 staining, but both showed worse IHC when increasing the delipidation time further. Incubation of tissue at 50°C for one hour prior to antibody incubation improved staining for Glut1 and NeuN. Glycine treatment had no significant effect on NeuN staining, but inhibited Glut1 staining. Incubating antibodies at RT improved NeuN staining and on Glut1 staining. Inclusion of PFA in the hydrogel resulted in decreased IHC quality for both Glut1 and NeuN,

however this significantly improved IHC of dopamine receptor 2 (**Figure S11**). Intriguingly, staining with DAPI appears insensitive to the different protocols (**Figure 2**). Therefore, we ascertained the optimal protocol for simultaneously staining Glut1, NeuN, and DAPI was to delipidate for 2 days, place the tissue at 50°C for 1 hour before incubating with antibodies, and incubating the antibodies at room temperature. Importantly, these same conditions would result in no staining of dopamine receptor 2 (**Figure S11)**. Instead, an IHC protocol is required to use PFA in the hydrogel step to show adequate staining of dopamine receptor 2, which can still allow for simultaneous staining of NeuN, Glut1, and DAPI if the tissue is only delipidated for one day and incubated with antibodies at 4°C . Together, these results show that different conditions can have opposite effects on the quality of staining and depth of antibody penetration and reinforce the importance of optimizing sample preparation conditions for each antibody.

Comparison of IHC conditions for different antibodies directed against a single protein

A common strategy following unsuccessful IHC in tissue is to test antibodies from different suppliers or antibodies raised against different epitopes in the desired target. To better understand whether optimal IHC protocols may be shared for antibodies against the same target, we compared the staining of a monoclonal GFAP directly conjugated to a fluorophore and a polyclonal GFAP that was detected with a fluorophore conjugated to a secondary antibody. To enable a direct comparison, both sets of antibodies were used to label the same tissue sections. Immunolabeling GFAP with different antibodies shows that the trends in staining quality are similar for both antibodies across all conditions (**Figure 3**). This suggests that conditions that enhance GFAP stability and prevent denaturation of its epitopes have a positive effect on all GFAP antibodies provided the antibodies are of high quality, have high specificity and limited off-target binding. This also suggests that IHC of GFAP with these antibodies is limited more by denaturation of the epitope than the antibody itself. Importantly, primary GFAP antibodies directly conjugated to a fluorophore showed significantly better penetration, signal-to-noise ratio, and less off-target staining for both GFAP antibodies under all conditions where IHC successfully labeled its target (**Figure 3**) and both showed similar conditions where no labeling occurred (**Figure s10)**. As this approach also reduces the length of the staining protocol, it is recommended to use primary antibodies directly conjugated to fluorophores whenever possible.

Multiple antibodies that recognize tau protein were also compared including AT8 anti-tau, HT7 anti-tau, and DAKO total tau antibodies. Tau is a microtubule associated protein that is primarily expressed by neurons and is the main component of neurofibrillary tangles in Alzheimer's disease. We chose three commonly used antibodies against tau and tested them first in tissue from a transgenic mouse model, hTau,[18] that expresses normal human tau isoforms. Importantly, when used in traditional immunohistochemistry in microtome slices of human tissue, all three of these antibodies labeled similar structures (**Figure S15**).

There was significantly more variability between tau antibodies than seen with GFAP antibodies, primarily due to the inability for DAKO total tau antibody to effectively penetrate the beyond the tissue's surface (**Figure 4**). However, as the DAKO total tau antibody was not directly conjugated to a fluorophore, we cannot exclude the possibility that the inability to image DAKO-stained tau beyond the surface may be an effect of poor penetration and diffusion of the secondary antibody. As expected, similar trends in optimal IHC protocols were observed for AT8 and HT7 anti-tau antibodies in mouse

tissue expressing human tau (**Figure S12**) and showed no labeling in a negative control; mice without tau expression (**Figure S13**).

Mouse brain tissue as a model system for optimizing IHC in cleared human tissue

Optimizing IHC in human tissue is especially difficult due to the limited amount of tissue available for experimentation. Therefore, we performed IHC optimization in both mouse and human brain tissue for individual antibodies and analyzed their similarities. Surprisingly, our testing of IHC protocols for NeuN and Glut1 in human tissue showed similar changes in staining quality and depth when compared to mouse tissue (**Figure 5**). Both human and mouse tissue showed decreases in staining quality with increasing clearing time and fixation with PFA. Room temperature antibody incubation as well as epitope unmasking at 50°C for 1 hour prior to antibody incubation improved Glut1 and NeuN staining in both mouse and human tissue. It is also worth noting that this NeuN antibody appears to accumulate off-target in the human tissue, which is not observed in the mouse tissue.

The optimal protocol that allows NeuN, Glut1, and AT8-tau staining was then determined by finding the conditions that allow for the simultaneous IHC of all three antibodies in a single tissue section, and then finding the combination of conditions among those that maximizing the staining quality. It is worth noting that this was not necessarily the best protocol for each individual antibody. It is more important to have adequate staining of each epitope than to have fantastic staining of one at the cost of another. As described above, we determined the optimal protocol for multiplexed labeling by combining the protocol changes that quantitatively improve the staining quality, defined by half-max depth, for each antibody above the baseline protocol and do not significantly degrade performance of other antibodies. For NeuN, Glut1, and AT8 antibodies this protocol involves clearing for 2 days, using 50°C to unmask epitopes, and incubation of antibodies at room temperature. The optimal protocol was then validated in 1mm thick pieces of human brain tissue, approximately 100-fold thicker than typical paraffin embedded sections. Antibodies for tau in mice expressing human tau show similar variability across conditions for the labeling of labeling tau in human tissue (**Figure 4**). As shown in Figure 3, the use of a primary antibody directly conjugated to a fluorophore greatly reduced background fluorescence over traditional primary/secondary antibody systems. Therefore, we directly conjugated three antibodies to three different fluorophores (NeuN-A568, Glut1-A488, and AT8-A647). These antibodies were used to stain tissue that was first embedded in a 4% acrylamide hydrogel, cleared for 2 days and thoroughly washed. The antibodies were incubated with the tissue for 14 days to ensure complete staining through the whole sample in both humans (**Figure 6**) and mice (**Figure S16**). It should be noted that we found 3 days of antibody incubation sufficient for consistent and thorough staining across brain regions in 500 µm mouse tissue (Figure S17, S18), and there were no notable downsides to leaving the antibody incubating longer. By carefully following the optimal IHC protocol determined in this work, we were able to achieve complete penetration and simultaneous labeling of the 1 mm thick human tissue with all three antibodies. Both the Glut1-labeled vasculature and AT8-labeled tau are extremely well defined and could be easily quantitated. The NeuN reflects the same quality that it had during the troubleshooting but does not appear to be an ideal antibody for assessment of human neurons under these conditions.

Discussion

Although it is well known that alterations to IHC protocols can have detrimental effects to the staining results, many researchers accept the dogma that a universal IHC protocol exists that is robust enough to

support labeling with a wide range of antibodies. When a subset of antibodies fail in a multi-target IHC protocol, often the antibodies themselves are blamed. Here, we have found that small changes to an IHC protocol can have profound effects on labeling efficiency. Rather than the antibody, our data suggests that poor staining is most often due to denaturation or blockage of the epitope. These procedural differences do not influence every antibody-antigen pair in the same way, so the optimal protocols for IHC should be determined for each individual target. Using combinations of antibodies in the same tissue may require using a protocol with conditions that are acceptable for all antibodies, rather than conditions that are optimal for each individual antibody. Unfortunately, as we found with the dopamine receptor 2 (**Figure S11)** and GFAP (**Figure 3, S10)** IHC, a protocol may not exist to allow for both targets to be effectively stained simultaneously. However, the methods described here allow a researcher to rapidly determine 1) an optimal protocol for single antibody staining, 2) an acceptable protocol that allows simultaneous multi-antibody staining or 3) that cyclical single-antibody staining and stripping will be required to match conditions necessary for each antibody.

Importantly, temperature, fixation conditions, and the other conditions investigated here have greater influence the larger the tissue volume becomes. For many of the tested protocols, the difference in staining is not apparent at the surface which suggests that the use of tissue sections that are too thin does not allow for appropriate optimization. Many of the protocols we tested for NeuN or Glut1 produce some degree of labeling at the surface of the sample that would have appeared no different between samples thinner than 50 µm, despite obvious differences in staining quality at depth.

Most surprising to us, was that mouse tissue is a good model system for determining large-volume IHC protocols for human samples. However, these results show minor procedural changes can disrupt the quality of staining, so it is important that tissue preparations are identical.

IHC protocols in large volume tissue that requires clearing can take weeks or months to complete depending on the initial state and size of the tissue.[10,19] Previous studies have suggested that human tissue requires processing for longer than comparable-sized rodent tissue. Our results suggest that this is not due to intrinsic differences between human and mouse brain tissue, but rather a result of differences in the state of the tissue when clearing experiments are started. Human tissue is often stored in fixative for extended periods of time and, as our data shows, even a small increase in PFA exposure can have significant influence on IHC quality and depth. To our surprise, tissue that was delipidated for three days showed less rapid IHC penetration than tissue that was cleared for 2 days in all cases except for DAPI labeling. This suggests that samples can quickly become over cleared and lose antigenicity which may extend the amount of time previously reported as necessary for IHC. It follows that future experiments should explore labeling tissue with antibodies with even shorter or milder fixation conditions and, where possible, carried out prior to any tissue clearing procedures.

Our methodology enables rapid optimization of IHC protocols, including protocols that require tissue clearing and provides a simple path to imaging tissue blocks that are 100 times thicker than conventional tissue slices. First, a library of cleared tissue samples that were each processed using different conditions is generated that can be stored for future experiments. Then, optimal IHC conditions are determined for new antibodies within a few days (approximately 24 hours for staining, 24 hours for rinsing, 12-24 hours for refractive index matching/clearing, 3 hours to image the samples, and a similar amount of time to quantify and compare the staining quality). The variability in staining quality across protocols suggest that researchers should use this process to test how changes may affect

antibodies or epitopes that they plan to study before committing many weeks or months to a procedure in larger volumes. Additionally, these results speak to the necessity for scientists to publish both conditions that improve and degrade specific antibody performance. Understanding which procedures and antibodies are appropriate for a given sample will be essential for tissue clearing techniques to gain widespread use in human tissue. We are optimistic that our optimization process will allow researchers use these techniques to successfully label cleared human tissue, which will improve the adoption of this technique and the ability to unlock new insight into human pathology and neuroanatomy.

Materials and Methods

Human tissue samples

Three human participants with AD were selected from the Massachusetts Alzheimer's Disease Research Center. Sex, age at death, Braak staging, which hemisphere, and comorbidities are listed in Supplementary Table 1. Autopsy tissue from human brains were collected at Massachusetts General hospital, with informed consent of patients or their relatives and approval of local institutional review boards. Human tissue was received immediately after autopsy and placed in 4% PFA for 48 hours at 4°C, transferred to PBS for 24 hours at 4°C before slicing. This tissue was treated identically to the mouse tissue described below in the tissue slicing procedure and onwards.

Mice strains

Male and female C57Bl/6J mice (Jackson Laboratory 000664) were used for most tissue experiments. For tissue to test IHC of tau, 10-12 month-old male hTau mice bred from a local colony (B6.Cg-Mapt$^{tm1(EGFP)Klt}$ Tg(MAPT)8cPdav/J, Jackson Laboratory 005491) that express only human tau isoforms were used. hTau knockout mice bred from a local colony (Mapt$^{tm1(EGFP)Klt)}$/J, Jackson Laboratory 004779) were used as controls for tau IHC experiments. Mouse experiments were performed with approval of local institutional review boards (IACUC protocol # 2019N000026).

Perfusion

Mice were transcardially perfused with ice-cold 40 ml phosphate-buffered saline (PBS), followed by 40 ml 4% paraformaldehyde (PFA, Electron Microscopy Sciences). Brains were removed from the cranium and placed in 4% PFA for 48 hours at 4°C. Brains were then transferred to PBS for 24 hours at 4°C before slicing.

Tissue slicing

Brains were embedded in 4% agarose hydrogel. To do this, extracted brains were placed individually in a small petri dish and let dry slightly. The agarose solution was dissolved by boiling in a microwave, then left on the counter to cool before pouring. Agarose was poured to completely cover the top of the brain, which allows it to provide a solid support to prevent deformation during cutting. A block of agarose containing the brain was placed in a vibratome (VT1000S vibrating blade microtome, Leica, Wetzlar, Germany) then cut into 500 or 1000 µm coronal or sagittal slices. Each slice was then removed from the agarose through gentle manipulation with blunt forceps or paintbrushes before crosslinking.

Tissue hydrogel crosslinking

Each slice was incubated with a hydrogel crosslinking solution for 1 day at 4°C to let the molecules diffuse through the tissue. Solutions should be kept cold before and after the addition of VA-044 to prevent premature initiation of polymerization. Different crosslinking solutions were used to determine the effect of including PFA on IHC. *Crosslinking solution 1*: PBS with 4% (wt/vol) acrylamide (Sigma-Aldrich, St. Louis, MO) and 0.25% (wt/vol) VA-044 thermal polymerization initiator (Fisher Scientific, Pittsburgh, PA). *Crosslinking solution 2*: PBS with 4% (wt/vol) acrylamide, 0.25% (wt/vol) VA-044 thermal polymerization initiator, and 4% PFA. After incubation with the crosslinking solution for 1 day, the tissue was left in solution and placed in vacuum at 37°C for 3 hours. After polymerization with X-CLARITY polymerization system (Logos Biosystems, South Korea), the slices were rinsed with 50 ml PBS three times over 3 hours. Each slice was then cut into small pieces with width and length at least twice the thickness. This was done to increase the number of conditions that could be tested with small amounts of tissue.

Delipidation

After hydrogel crosslinking, the tissue was placed in a delipidation solution (SDS 200 mM, Sodium sulfite 20mM, Sodium Borate 20mM, Sodium Hydroxide to pH 8.5-9. Filtered if necessary) at 37°C for different amounts of time (1, 2, or 3 days), to determine the effect of delipidation in IHC. After delipidation, the brain slices were rinsed with 50 ml PBST (PBS with 0.2% Triton X-100, Thermo Fisher Scientific) five times over 1 day.

Pre-immunohistochemistry tissue processing

Different conditions were tested at this step to determine their influence on immunohistochemistry. Each tissue section was tested using only one of the following conditions. *Baseline:* Tissue was left at 4°C in PBST. *50°C Condition:* Tissue was heated to 50°C for 1 hour in PBST. *Glycine:* Tissue was incubated with 0.1 M Glycine at 4°C for 12-18 hours. *Glycerol:* Tissue was placed in a low osmolarity solution of 80% glycerol/20% water for 12-18 hours. *Blocking:* Tissue was placed in 5% BSA in PBS for 12-18 hours.

Storage of tissue library

The tissue library was then used immediately or stored at 4°C in PBS with 0.02% (w/v) sodium azide. Mouse and human tissue was processed following all of the steps above and then used up to 3 months later. Additional mouse and human tissue was stored following delipidation, then successfully used up to 6 months later by resuming from the pre-immunohistochemistry tissue processing state. IHC conditions for a given antibody were always compared using batches of tissue that were stored for the same amount of time.

Immunohistochemistry

- The following antibodies were purchased then stored according to the vendors specifications: NeuN antibody conjugated to Alexa Fluor 568 (Abcam, Ab207282).
- GFAP antibody unconjugated (Abcam, ab16997) and conjugated to Alexa Fluor 488 (Thermo Fisher, 53-9892-82).
- Glut1 antibody conjugated to Alexa Fluor 488 (EMD Millipore, 07-1401-AF488).
- Phospho-Tau antibody AT8 conjugated to biotin (Thermo Fisher, MN1020B).
- Tau monoclonal antibody HT7 conjugated to Alexa Fluor 647 (Thermo Fisher, 51-5916-42).
- DAKO total tau antibody unconjugated (Agilent, A0024).

- Dopamine Receptor 2 antibody (Santa Cruz Biotechnology, SC5303)
- Secondary antibody Goat Anti-Rabbit IgG H&L conjugated to Alexa Fluor 405 (Abcam, ab175652) and Alexa Fluor 647 (ab150079).
- Streptavidin conjugated to Alexa Fluor 568 (Thermo Fisher, S11226).

Each brain slice was placed in a 2 ml Eppendorf tube (or similar vessel) that could hold the slice so its large, flat sides could be exposed to solution. PBST was added to just cover the top of the samples (~300 µl). 1-5 µl of stock antibody solution was added, depending on the concentration of the stock. The final concentration of each antibody in solution was 5 µg/ml. Fluorophores or host species were chosen so multiple different antibodies could be tested at the same time in a single slice of tissue. The tissue was then incubated with the antibodies at 4°C or room temperature for 18 hours. The tissue was then rinsed in PBST 3x 50ml overnight (18-24 hours) at room temperature. If using unconjugated primary antibodies, the secondary antibodies were then added to give a final concentration of 5 µg/ml and incubated for 48 hours at 4°C. The tissue was then rinsed in PBST 3x 50ml overnight at room temperature.

IHC of human microtome sections

Prior to preparation of cleared tissue volumes, fresh/frozen human samples were tested for the presence of AT8, HT7, and DAKO. Microtome sections were fixed in 4% PFA for 15 minutes, rinsed in Tris-buffered saline (TBS) three times, then blocked in TBS with 5% bovine serum albumin. Primary antibodies were incubated at a concentration of 1:500 overnight. Tissue was rinsed in TBS 3x, then incubated in secondaries at room temperature for 60 minutes, and rinsed in TBS 3x. Immumount was then used to seal the tissue prior to imaging.

Refractive index matching

The samples were incubated with 80% glycerol, 15% DI water, 5% PBS (RI-matching solution) for at least 3 hours at RT with gentle shaking. The RI-matching solution was then replaced with fresh solution and left to incubate for at least 3 more hours before imaging. Samples were stable stored in this solution at room temperature and could be re-imaged for at least 3 months.

Imaging

Samples were imaged using Olympus Inverted Confocal FV3000 with a 10x objective except for samples using dopamine receptor antibodies which were imaged using the Zeiss Lightsheet Z.1. Image Z-stacks were then reconstructed and visualized using Imaris microscopy image analysis softwhere.

Post-imaging analysis

Prior to analysis, images were assigned a random number so the analyzing scientist was blind to tissue clearing conditions but still aware of the antibodies used in the tissue, which was necessary to identify staining.

Analysis with Imaris

Imaris software was used to assess the staining quality score. First, the distribution of fluorescence values across all slices in the z-stack were normalized. Then, a rolling ball algorithm was applied to define the edges of fluorescent shapes with signal intensity greater than background by a threshold value. The area within each slice of a z-stack that contained staining above this threshold was then

divided by the maximum across all tissue stained with that fluorophore to determine the staining quality throughout the tissue. This metric was only applied to stains like NeuN or Glut1 in the cortex where we can make the assumption that there is a uniform and consistent distribution of these cells across sections. All samples that were imaged as part of the library described in Scheme 1 were included in this study, with at least 3 independent samples per condition to determine reproducibility.

Analysis with Ilastik

Raw data was converted to HDF5 format using ilastik's ImageJ plugin plus custom macro to batch convert. The staining was then segmented using their pixel classifier workflow[20]. In short, a paintbrush was used to draw over the signal and background to help train the classifier on how to segment each image. Real-time segmentation results were then improved using a minimum of 600 image planes from 6 different staining conditions that reflect the distribution of staining quality in the entire set. All images were then batch processed through the trained pixel classifier and exported as multi-page tiff.

Post-Image-segmentation analysis in Matlab

The image segmentation output from either Imaris or Matlab was saved as a single-channel multipage Tiff and placed into a folder, and all the raw images were saved as a single-channel multipage Tiff and placed into a different folder. Image conversion was done using ImageJ macros. Quantification and generation of data for plotting can then be done by specifying the data path, ensuring the matlab code is on the path, then running the code. The main code "QuantifyIHC.mat" should be run first, which goes through the files in each folder in order and determines the segmentation area, staining within the segmentation, and noise outside of the segmentation. Next, running the "FindHalfHax.mat" code will find the starting plane for plotting, the half-max depth, place all data for plotting into arrays, allow for the re-ordering of blinded data, and plotting of the heatmaps.

Data availability

All data used in publication can be accessed at the BioImage Archive https://www.ebi.ac.uk/biostudies/studies/S-BIAD479.

Code availability

All Matlab code and ImageJ macros used to quantify data can be accessed at https://github.com/tjzwang/IHC.

Acknowledgements

This work was supported by the NIH/NIA-K99AG068602 (T.J.Z.) and the Harrison Gardner, Jr. Award (T.J.Z)

We would like to thank Massachusetts General Hospital Center for comparative Medicine and Analiese Fernandes for help with animal husbandry and care. We would also like to thank the Harvard Center for Biological Imaging including Christian Hellriegal for the use of their imaging facility and helpful conversations. Autopsy tissue from human brains were collected at Massachusetts General hospital, with informed consent of patients or their relatives and approval of local institutional review boards.

Author Information

Contributions

T.J.Z. designed the study and performed most of the experiments and analysis. T.J.Z., A.Z., C.M.L, R.E.B., D.C.R. and B.T.H. conceived of experiments. T.J.Z., M.L., R.E.B., and B.W. performed tissue collection, preparation, staining, and imaging. All authors discussed the results and commented on the manuscript text.

Corresponding author

Correspondence to Theodore J. Zwang (tzwang@mgh.harvard.edu)

Competing Interests

The authors declare no competing interests.

References

1) Ueda, H.R., Ertürk, A., Chung, K. *et al.* Tissue clearing and its applications in neuroscience. *Nat Rev Neurosci* **21,** 61–79 (2020).
2) Richardson DS, Guan W, Matsumoto K, et al. TISSUE CLEARING. *Nat Rev Methods Primers*. **1**, 84 (2021)
3) Kim SW, Roh J, Park CS. Immunohistochemistry for Pathologists: Protocols, Pitfalls, and Tips. *J Pathol Transl Med*. **50**, 411-418 (2016)
4) Murray E, Cho JH, Goodwin D, et al. Simple, Scalable Proteomic Imaging for High-Dimensional Profiling of Intact Systems. *Cell*. **163**, 1500-1514. (2015)
5) Yun, D.H., Park, Y-G., Cho, J.H. *et al.* Ultrafast immunostaining of organ-scale tissues for scalable proteomic phenotyping *BioRxiv* doi: https://doi.org/10.1101/660373 (2019)
6) Na, M., Kim, K., Lim, H. R., Ha, C. M. & Chang, S. Rapid immunostaining method for three-dimensional volume imaging of biological tissues by magnetic force-induced focusing of the electric field. Brain Struct. Funct. 226, 297–309 (2021).
7) Dwyer, J., Ramirez, M. D., Katz, P. S., Karlstrom, R. O. & Bergan, J. Accelerated clearing and molecular labeling of biological tissues using magnetohydrodynamic force. Sci. Rep. 11, 16462 (2021)
8) Marina, S., Luca P., Niamh b. *et al.* Comparison of Different Tissue Clearing Methods for Three-Dimensional Reconstruction of Human Brain Cellular Anatomy Using Advanced Imaging Techniques. *Front. Neuroanat.* **15** (2021)
9) Lai, H.M., Liu, A.K.L., Ng, H.H.M. *et al.* Next generation histology methods for three-dimensional imaging of fresh and archival human brain tissues. *Nat Commun* **9,** 1066 (2018)
10) Susaki, E.A., Shimizu, C., Kuno, A. *et al.* Versatile whole-organ/body staining and imaging based on electrolyte-gel properties of biological tissues. *Nat Commun* **11,** 1982 (2020)
11) Matos LL, Trufelli DC, de Matos MG, da Silva Pinhal MA. Immunohistochemistry as an important tool in biomarkers detection and clinical practice. *Biomark Insights*. **5**, 9-20 (2010)
12) Zhao et al., Cellular and Molecular Probing of Intact Human Organs. *Cell*. 2020
13) Richardson DS, Lichtman JW. Clarifying Tissue Clearing. Cell. **162**, 246-257 (2015)
14) Shi S-R, Shi Y, Taylor CR. Antigen Retrieval Immunohistochemistry: Review and Future Prospects in Research and Diagnosis over Two Decades. *Journal of Histochemistry & Cytochemistry*. **59**, 13-32 (2011)

15) Wassie, A.T., Zhao, Y. & Boyden, E.S. Expansion microscopy: principles and uses in biological research. *Nat Methods* **16**, 33–41 (2019)
16) Park, YG., Sohn, C., Chen, R. *et al.* Protection of tissue physicochemical properties using polyfunctional crosslinkers. *Nat Biotechnol* **37,** 73–83 (2019)
17) Muratov EN, Bajorath J, Sheridan RP et al. QSAR without borders. *Chem Soc Rev.* **49**, 3525-3564 (2020)
18) Andorfer C, Kress Y, Espinoza M *et al*. Hyperphosphorylation and aggregation of tau in mice expressing normal human tau isoforms. *J Neurochem*. **86**, 582-90 (2003)
19) Ueda, H.R., Dodt, H.-U., Osten, P. et al. Whole-Brain Profiling of Cells and Circuits in Mammals by Tissue Clearing and Light-Sheet Microscopy. *Neuron.* **106**, 369-387 (2020)
20) Berg S., Kutra D., Kroeger T *et al.* ilastik: interactive machine learning for (bio)image analysis *Nature Methods* **16**, 1226-1232 (2019)

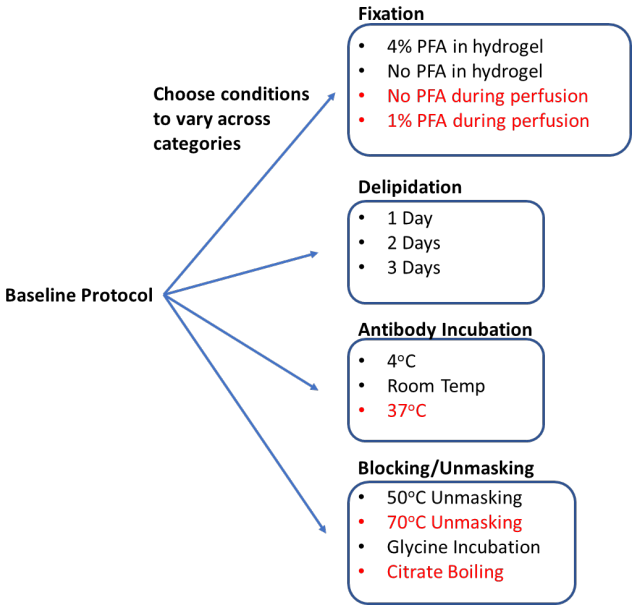

Scheme 1. Process for generating a library of tissue prepared with different protocols. Start with a baseline protocol (see Methods). Choose conditions to test that can be separated into categories believed to influence staining quality. Prepare tissue by varying only one or two conditions from the baseline at a time, so resulting IHC quality can isolate the effect of each condition change. Stored library of cleared tissues then allows for rapid antibody testing to quickly determine optimal IHC conditions for each antibody as well as protocols that allow for multiplexed IHC. We consistently found conditions in red to have exclusively negative effects on IHC or tissue integrity, so they were excluded from testing with most antibodies.

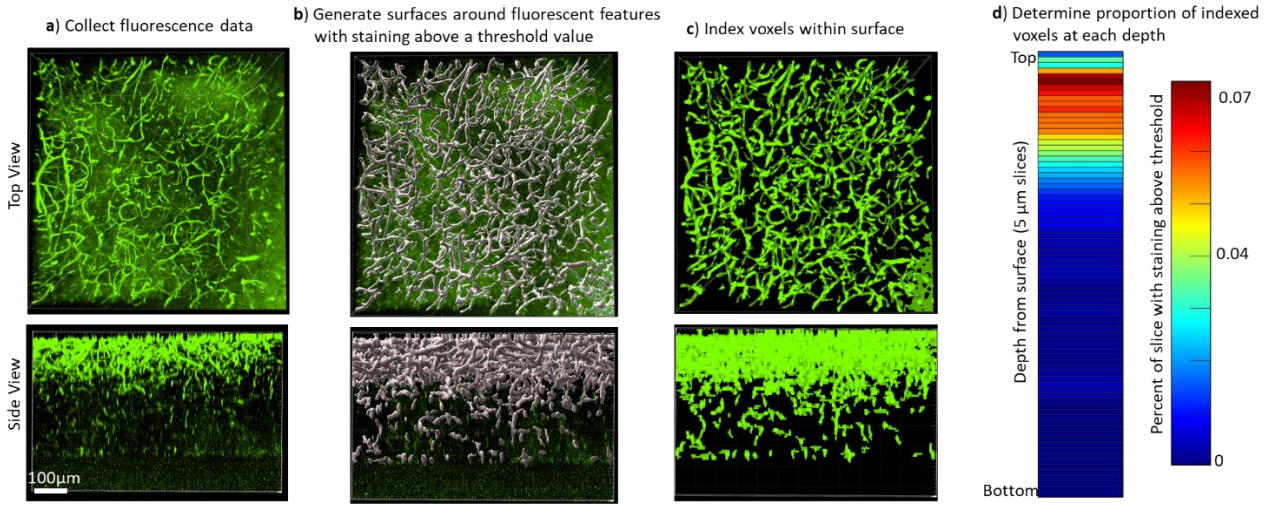

Scheme 2. Quantifying the staining quality for comparison across protocols and antibodies. IHC quality comparisons can be difficult to determine by eye due to differences in fluorescence intensity and background, as well as the many ways that software can modify the visual representation of data, so we created a pipeline to quickly quantify staining quality in a way that allows rapid comparison. **a** First, a confocal or lightsheet microscope is used to image a Z-stack throughout the entire thickness of the sample. All imaging parameters are kept identical for a given antibody/fluorophore to allow for comparison between protocols. **b** Fluorescence values were normalized across the sample, then a rolling-ball algorithm was used in Imaris software to generate surfaces around fluorescent features with intensity above a threshold value. Alternatively, segmentation masks were generated using Ilastik following their pixel classifier workflow. **c** The voxels within the surface were indexed to define the array of voxels with and without staining that could then be analyzed in Matlab. **d** The staining quality was quantified and visualized by plotting the ratio of voxels with staining over the total number of voxels in a plane at that depth in the image, the average signal intensity within the segmented region, and the average noise intensity outside of the segmented region (Figures S2, S3, S4, S5). A higher proportion of indexed voxels, higher signal, lower noise, and longer depth to reach half-max staining intensity all represent better staining quality. This can also be used to provide visual representation of reproducibility. (Fig S6, S7, S8) It is also possible to reduce these numbers into a figure of merit that can be quantitatively compared between conditions (Fig 1c, Fig S9).

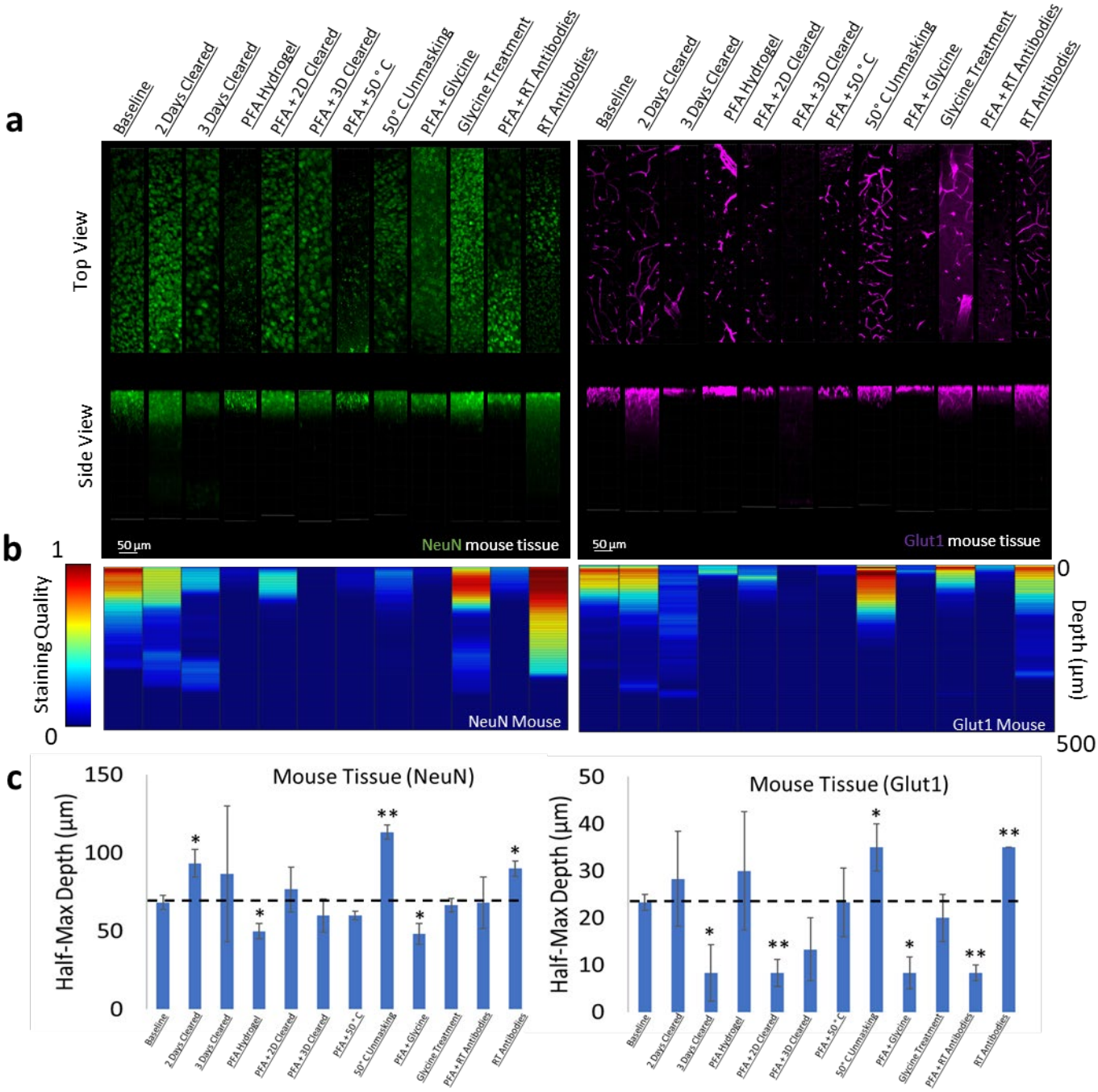

Figure 1. Influence of common conditions on immunohistochemistry in mouse brain tissue. a Representative maximum intensity projection views from the top and side of 500µm thick, 5mm wide tissue sections. C57Bl/6J mouse isocortex was processed, stained, and imaged simultaneously with NeuN (green, left panels) and Glut1 (purple, right panels). **b** Quantitative comparison of immunohistochemistry labeling across conditions using Imaris. A rolling-ball subtraction was used to determine the area with signal-to-noise above cut-off for every image plane in the Z-stack. The proportion of indexed voxels in each plane was then divided by the maximum value across all conditions to generate a normalized staining quality score, which allows for quick visual assessment of staining

quality differences with depth and between conditions. **c** Quantitative comparison of the depth at which the IHC staining intensity becomes half of the maximum, using segmentation results from Ilastik. Error bars represent standard error. Two-tailed t-test comparing results to baseline were represented with p <.05 = * , p <.01 = ** ,and no significance = unlabeled. N=3 for all samples.

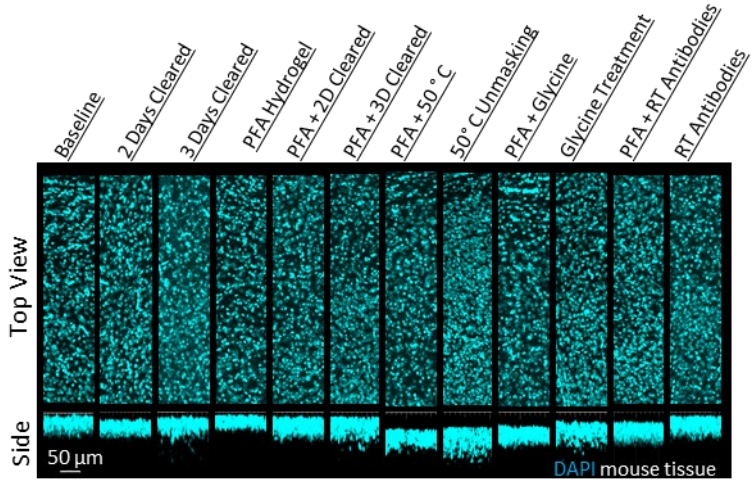

Figure 2. Influence of common conditions on DAPI staining. Representative maximum intensity projection views from the top and side of 500µm thick, 5mm wide tissue sections of C57Bl/6J mouse isocortex stained with DAPI.

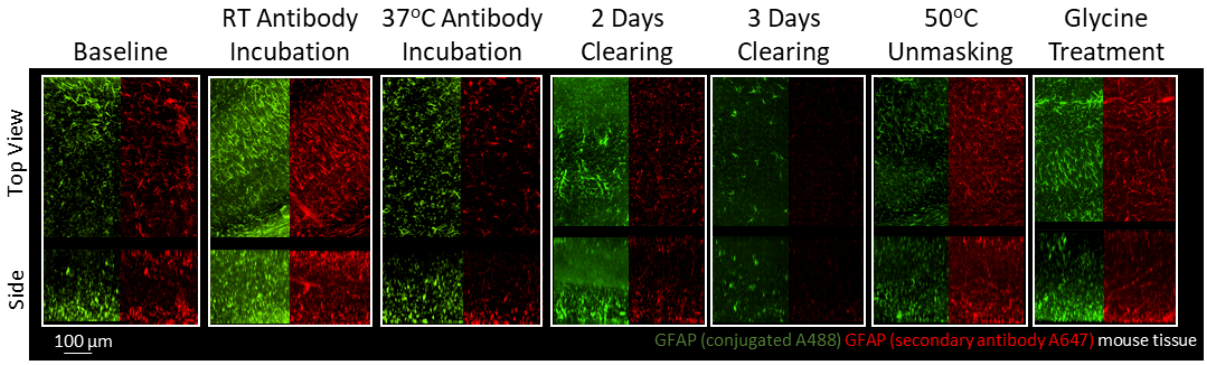

Figure 3. Immunohistochemistry of two different antibodies for GFAP. Representative maximum intensity projection views from the top and side of 500µm thick, 5mm wide tissue sections of C57Bl/6J mouse isocortex stained with two different antibodies for GFAP. Monoclonal GA5 conjugated to Alexa Fluor 488 (green) was stained and imaged in the same tissue as a polyclonal antibody using a goat anti-rabbit secondary conjugated to Alexa Fluor 647 (red). Other protocols show no significant labeling (S10).

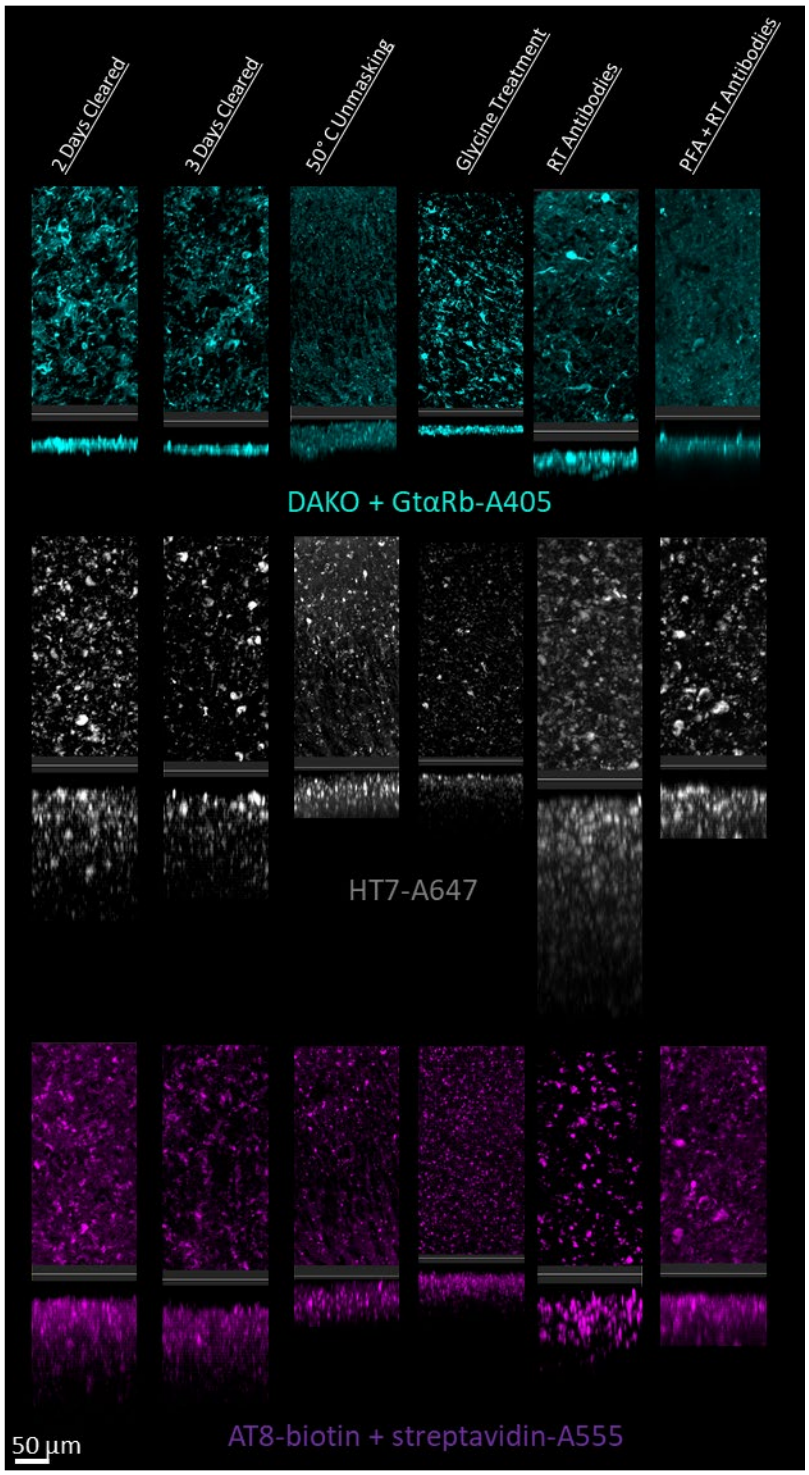

Figure 4. Tau immunohistochemistry in cleared human tissue. Representative maximum intensity projection views from the top and side of 500µm thick, 5mm wide tissue sections. Other protocols showed worse staining quality (Figure S14)

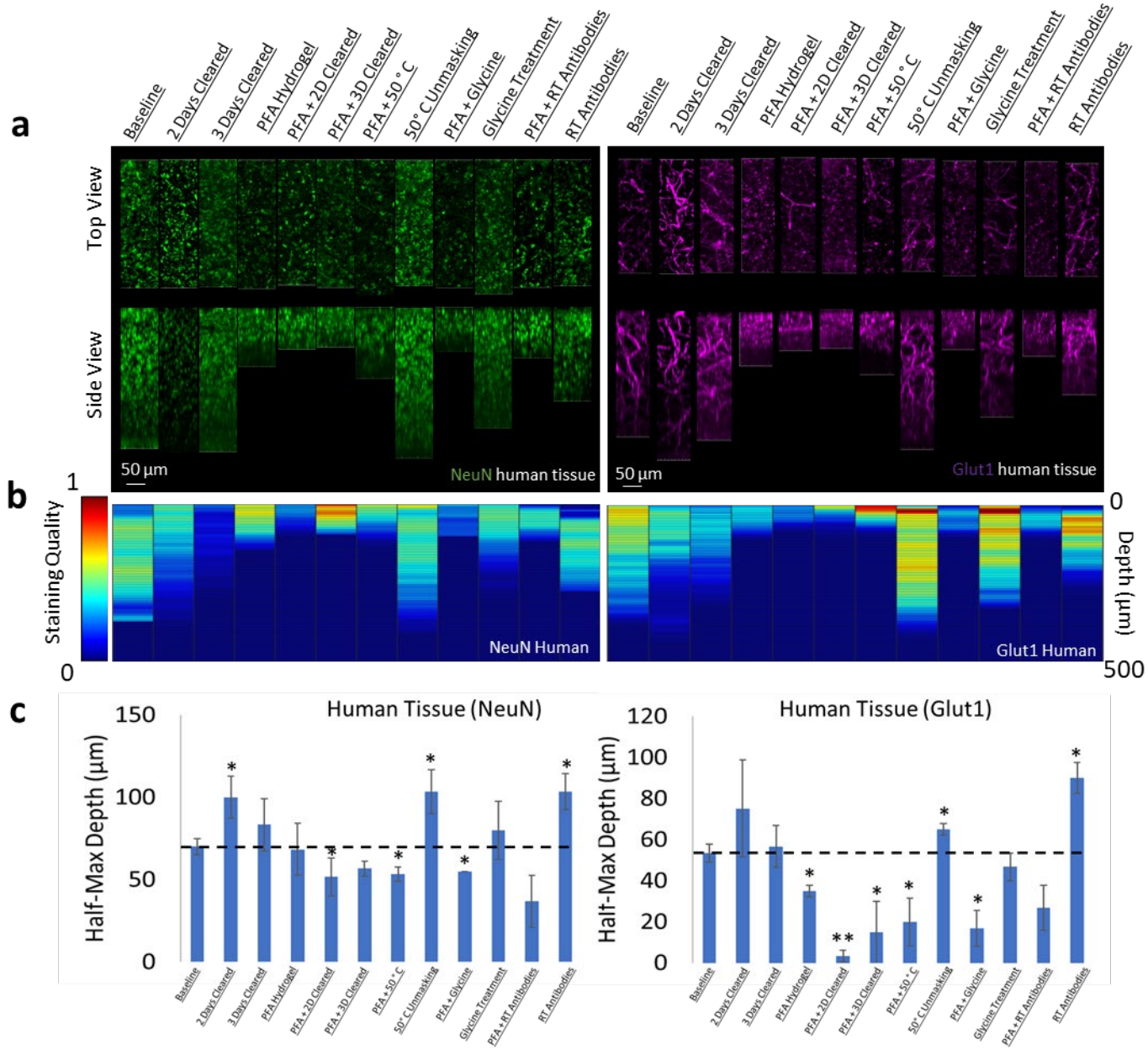

Figure 5. Influence of common conditions on immunohistochemistry in human brain tissue. a Representative maximum intensity projection views from the top and side of 500µm thick, 5mm wide tissue sections. Tissue was processed, stained, and imaged simultaneously with NeuN (green, left panels) and Glut1 (purple, right panels). **b** Quantitative comparison of immunohistochemistry labeling across conditions using Imaris. A rolling-ball subtraction was used to determine the area with signal-to-noise above cut-off for every image plane in the Z-stack. The area in each plane was then divided by the maximum value across all conditions to provide a staining quality score, which allows for quick visual assessment of staining quality differences with depth and between conditions. **c** Quantitative comparison of the depth at which the IHC staining intensity becomes half of the maximum, using segmentation results from Ilastik.

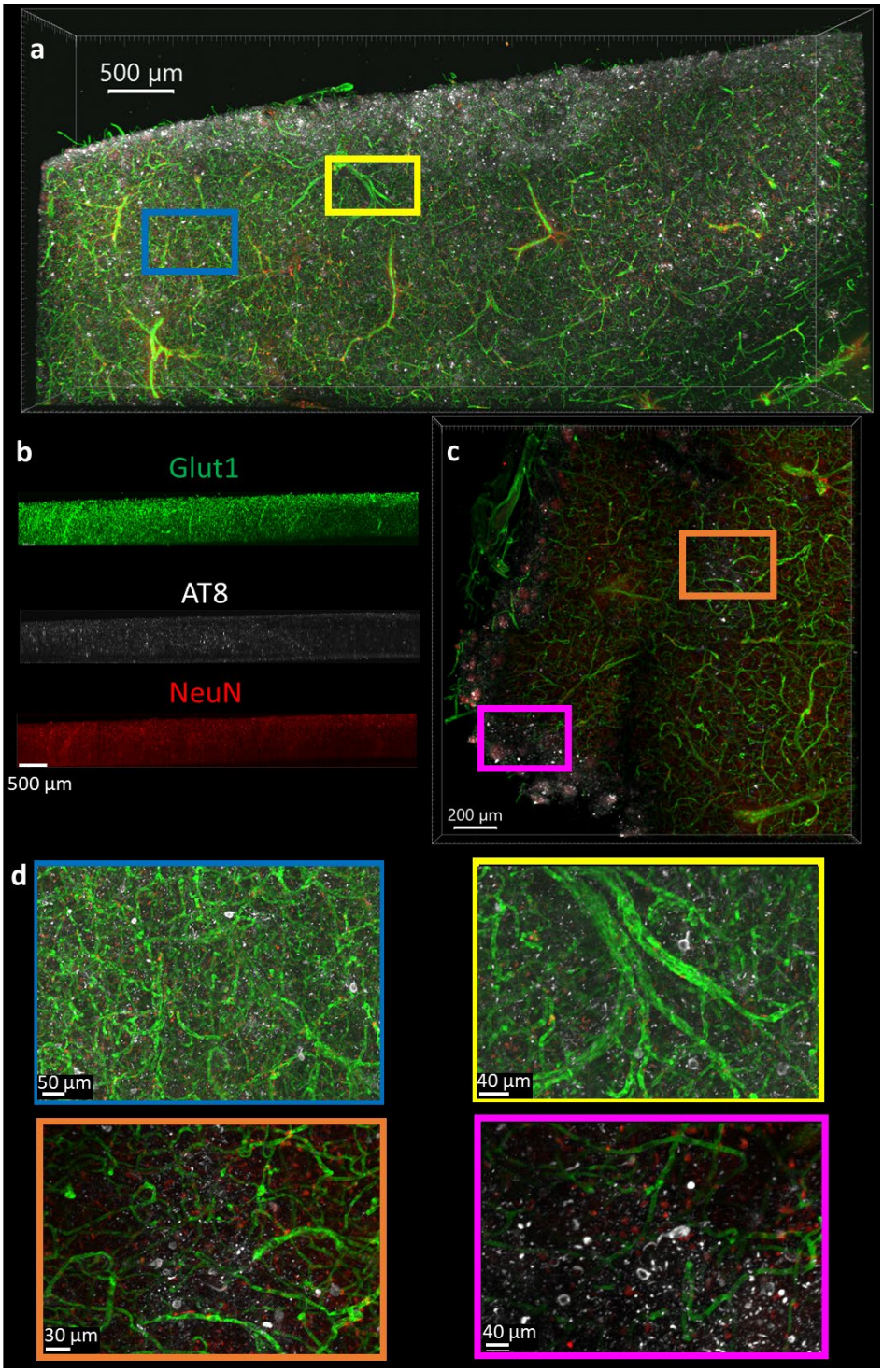

Figure 6. Immunohistochemistry in 1 mm thick human tissue. The tissue was crosslinked without PFA, cleared for 2 days, rinsed, then the antibodies NeuN-A568 (Red), Glut1-A488 (Green), and AT8-A647 (White) were incubated with the tissue for 14 days. **a** Top-down view of fluorescence from 1mm section

human brain. **b** Side view of each antibody fluorescence through entire section depth. **c** A 200 µm virtual section of human tissue, from a 1mm thick sample. **d** Zoomed-in regions from the full images show AT8-labeled tau tangles are present at multiple locations throughout the human brain sections.

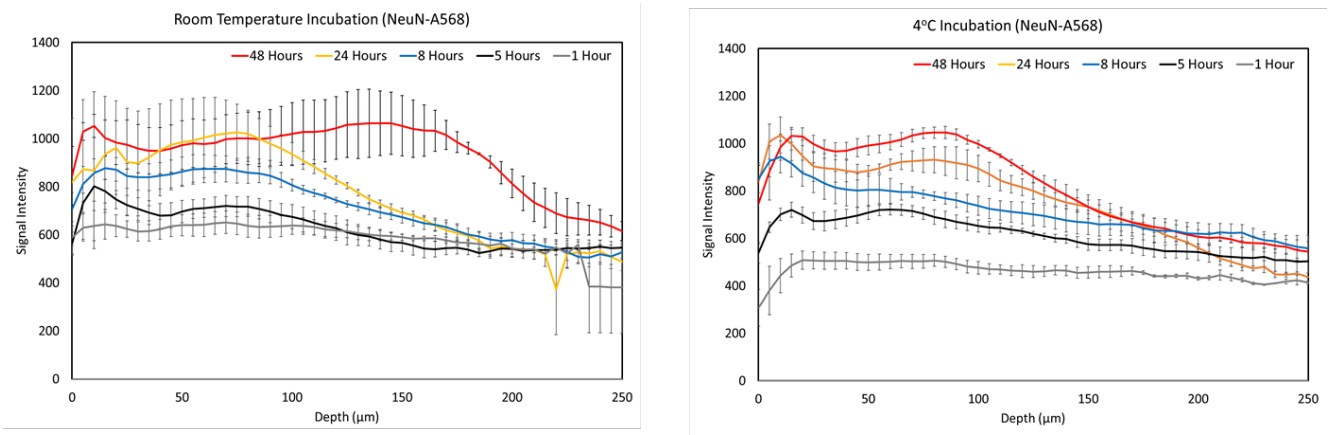

Figure S1. Immunohistochemistry staining depth over time. Average signal intensity of immunohistochemistry labeling with NeuN-A568 in mouse cortex tissue prepared using baseline conditions, with antibodies incubated at room temperature (left) and 4oC (right) with gentle shaking. For each time point, n = 3 independently prepared sections from different mice

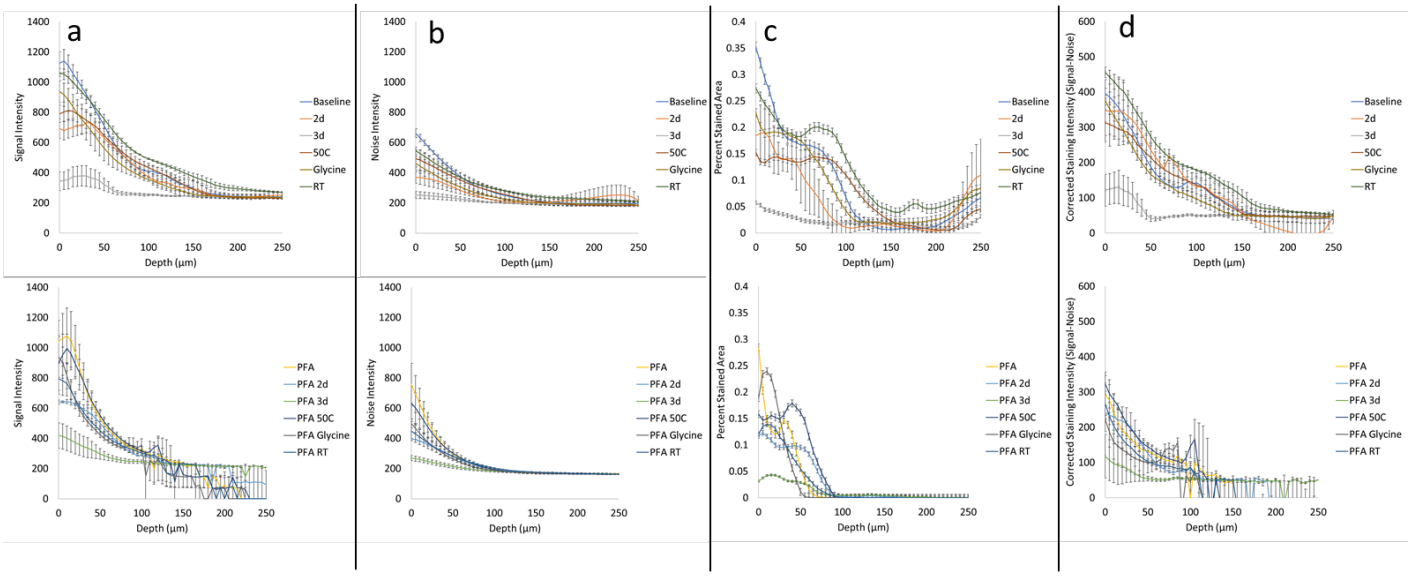

Figure S2. Immunohistochemistry performance of NeuN in mouse tissue. Quantification of the **a** average signal intensity, **b** average background noise intensity, **c** percent of segmented area, **d** and the average corrected staining intensity versus depth from the tissue surface. Signal, noise, and corrected signal were normalized to the amount of staining in each imaging plane by dividing the percent segmented area in that plane. Immunohistochemistry labeling was conducted with NeuN-A568 in mouse cleared tissue library with 3 independently prepared sections from different mice for each condition.

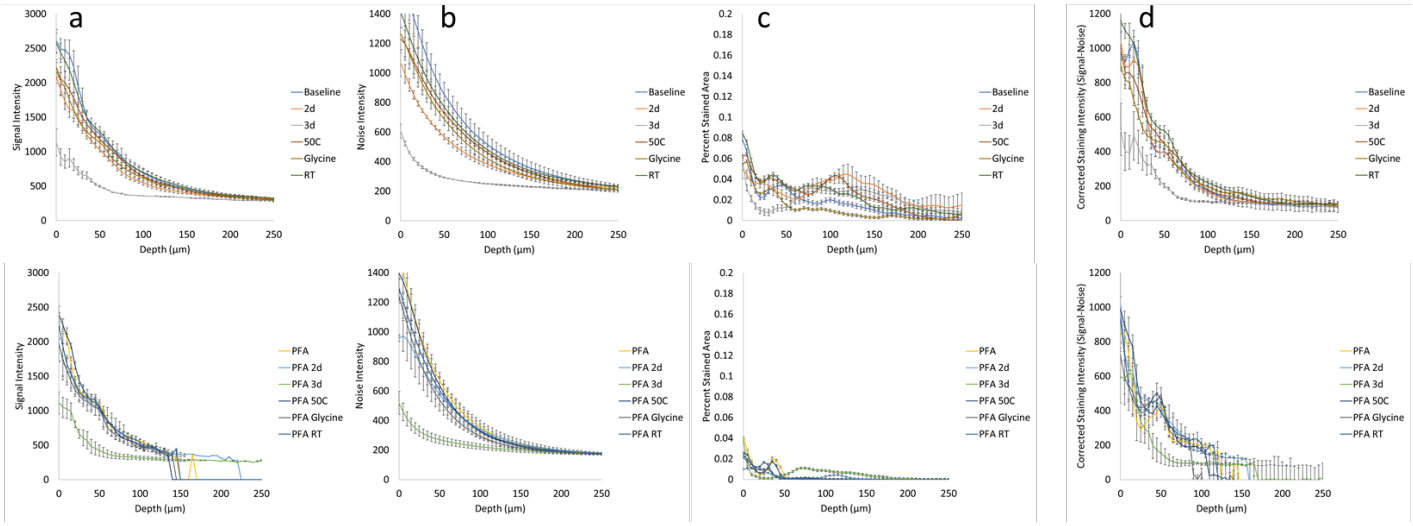

Figure S3. Immunohistochemistry performance of Glut1 in mouse tissue. Quantification of the **a** average signal intensity, **b** average background noise intensity, **c** percent of segmented area, **d** and the average corrected staining intensity versus depth from the tissue surface. Signal, noise, and corrected signal were normalized to the amount of staining in each imaging plane by dividing the percent segmented area in that plane. Immunohistochemistry labeling was conducted with Glut1-A568 in mouse cleared tissue library with 3 independently prepared sections from different mice for each condition.

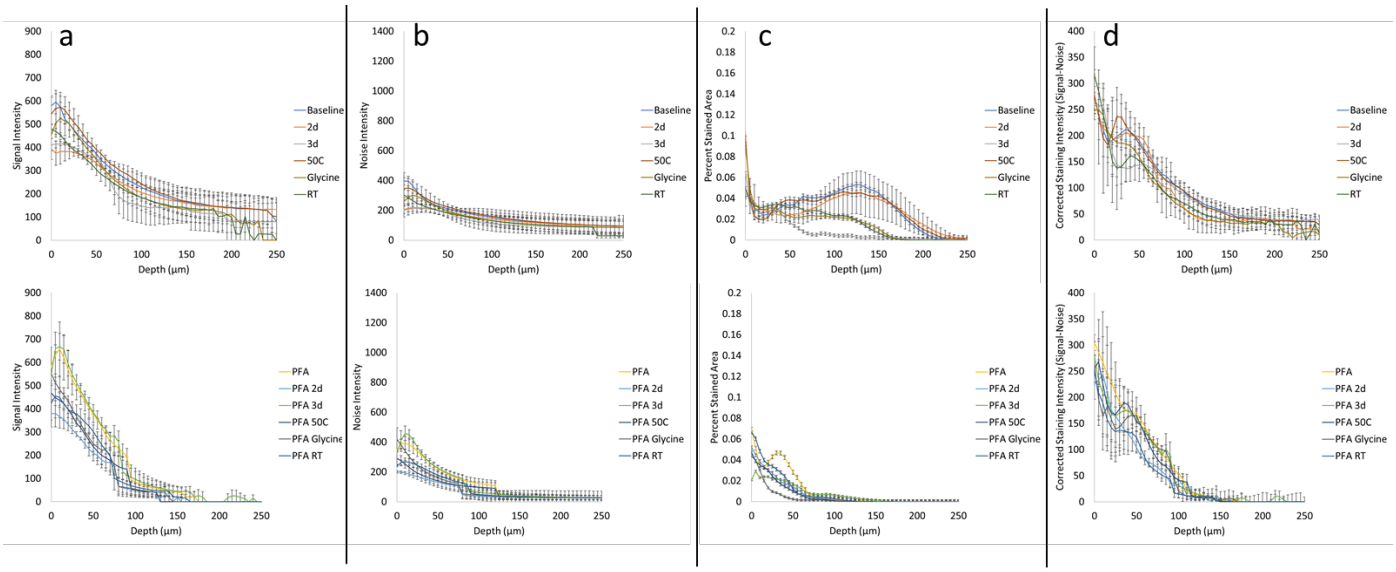

Figure S4. Immunohistochemistry performance of NeuN in human tissue. Quantification of the **a** average signal intensity, **b** average background noise intensity, **c** percent of segmented area, **d** and the average corrected staining intensity versus depth from the tissue surface. Signal, noise, and corrected signal were normalized to the amount of staining in each imaging plane by dividing the percent segmented area in that plane. Immunohistochemistry labeling was conducted with NeuN-A568 in human cleared tissue library with 3 independently prepared sections from different donors for each condition.

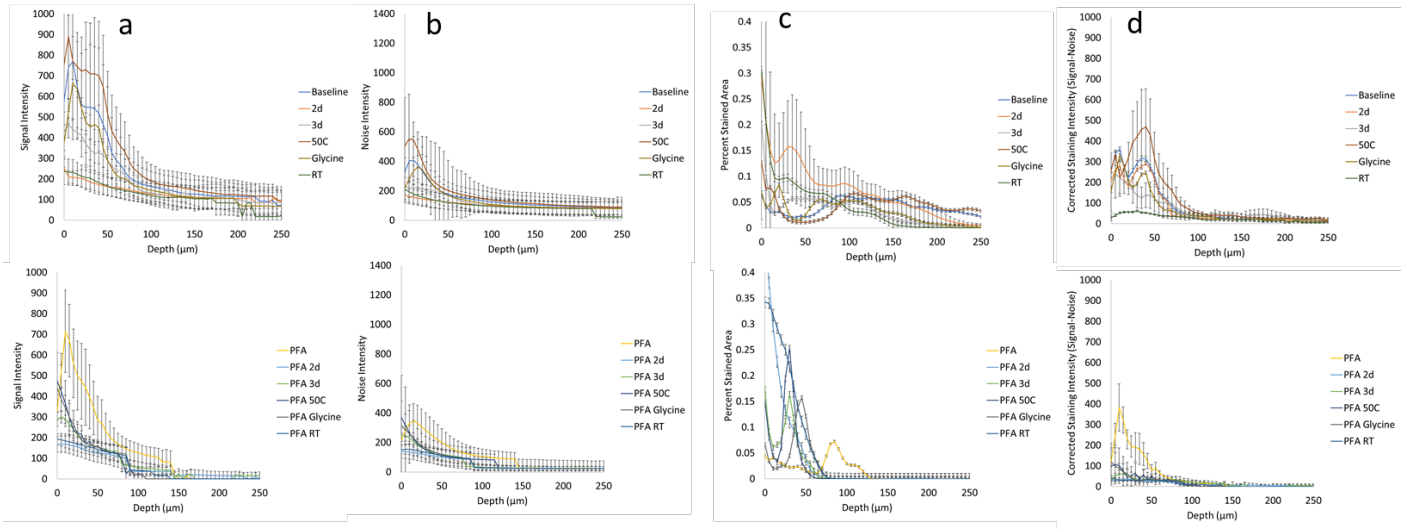

Figure S5. Immunohistochemistry performance of Glut1 in human tissue. Quantification of the **a** average signal intensity, **b** average background noise intensity, **c** percent of segmented area, **d** and the average corrected staining intensity versus depth from the tissue surface. Signal, noise, and corrected signal were normalized to the amount of staining in each imaging plane by dividing the percent segmented area in that plane. Immunohistochemistry labeling was conducted with Glut1-A488 in human cleared tissue library with 3 independently prepared sections from different donors for each condition.

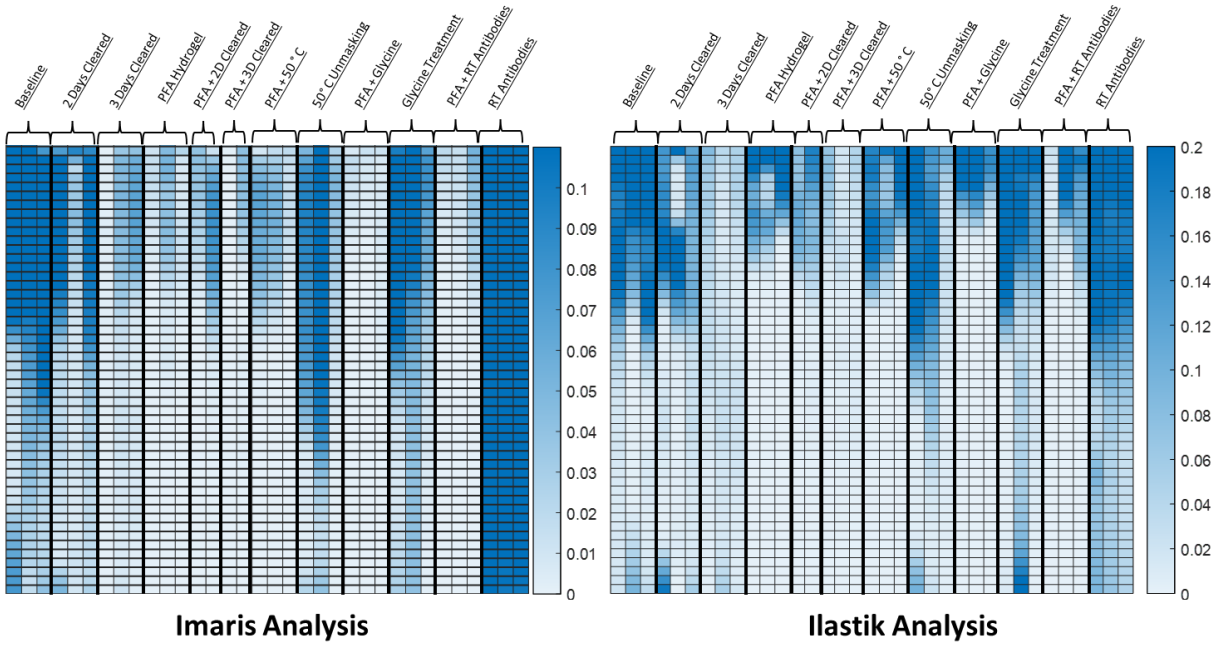

Figure S6. Reproducibility of NeuN immunohistochemistry and analysis in mouse brain tissue. Quantitative comparison of immunohistochemistry labeling across conditions. N = 3 independently prepared tissue sections from different mice for each condition. All conditions were tested with one section each from the same three mice. (left) For the Imaris analysis A rolling-ball subtraction was used to determine the area with signal-to-noise above cut-off for every image plane in the Z-stack. (right) For the Ilastik analysis, the staining was segmented using their pixel classifier workflow. In short, a paintbrush was used to draw over the signal and background to help train the classifier on how to segment each image. Real-time segmentation results were then improved using a minimum of 600 image planes from 6 different staining conditions that reflect the distribution of staining quality in the entire set. All images were then batch processed through the trained pixel classifier.

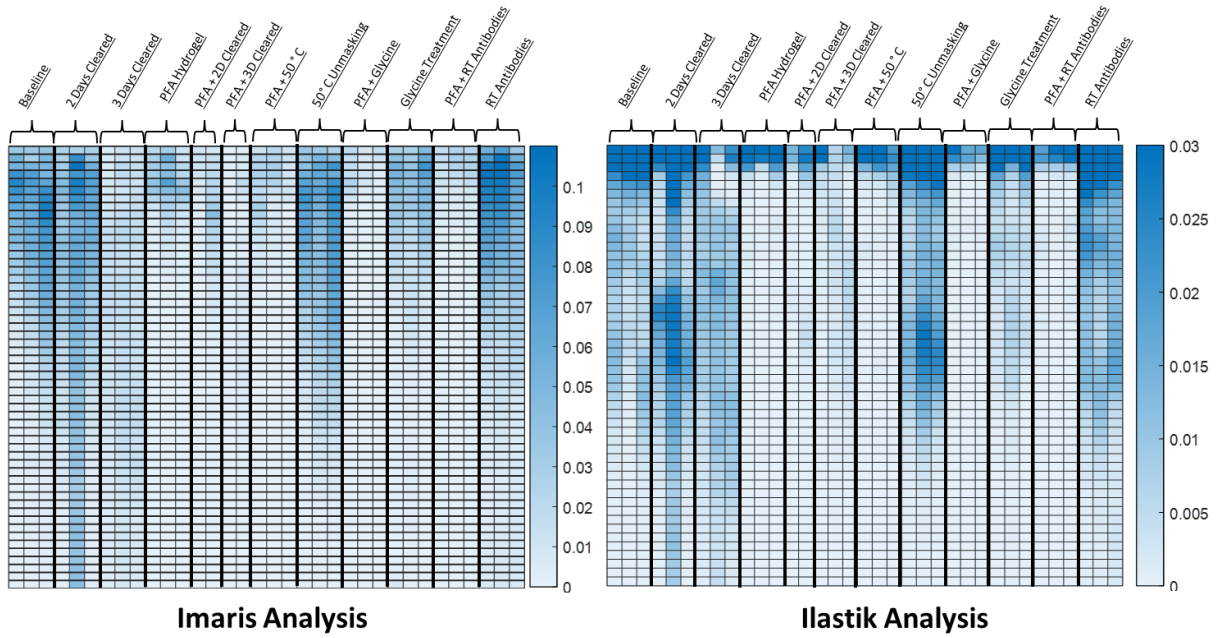

Figure S7. Reproducibility of Glut1 immunohistochemistry and analysis in mouse brain tissue
Quantitative comparison of immunohistochemistry labeling across conditions. N = 3 independently prepared tissue sections from different mice for each condition. All conditions were tested with one section each from the same three mice. with each condition having every condition having . (left) For the Imaris analysis A rolling-ball subtraction was used to determine the area with signal-to-noise above cut-off for every image plane in the Z-stack. (right) For the Ilastik analysis, the staining was segmented using their pixel classifier workflow. In short, a paintbrush was used to draw over the signal and background to help train the classifier on how to segment each image. Real-time segmentation results were then improved using a minimum of 600 image planes from 6 different staining conditions that reflect the distribution of staining quality in the entire set. All images were then batch processed through the trained pixel classifier.

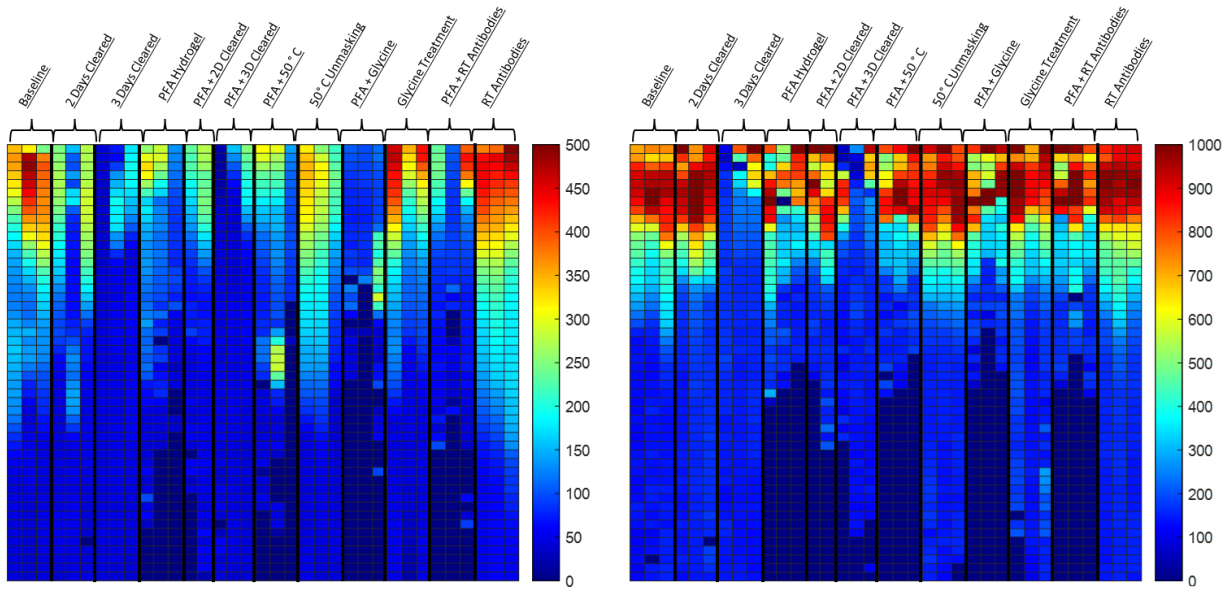

Mouse Tissue (NeuN)

Figure S8 Reproducibility of NeuN and Glut1 immunohistochemistry corrected signal intensity in mouse brain tissue. Segmentation results from ilastik were used to determine the signal within the segmented area as well as the noise outside of the segmented area. The noise values were subtracted from the signal value to visually represent the staining intensity value over noise. These change with depth in a notably different way than the segmented area (Figure S5, Figure S6) which suggests that conditions differentially influence the amount of staining and the intensity of staining.

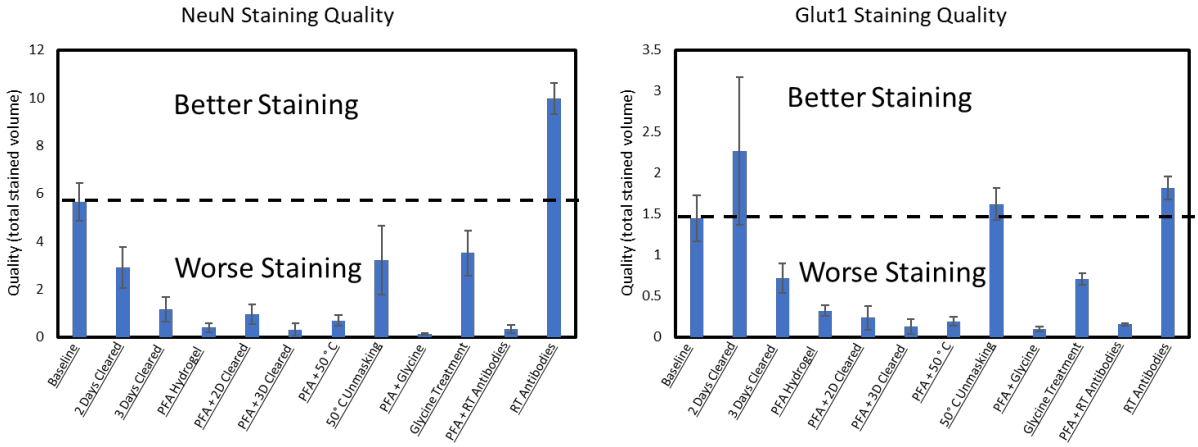

Figure S9. Reducing comparison of total stained volume to one-dimension. Quantitative comparison of immunohistochemistry labeling across conditions using Imaris analysis. A rolling-ball subtraction was used to determine the area with signal-to-noise above cut-off for every image plane in the Z-stack. The total area in each plane with fluorescence above the threshold value was them summed to reduce the dimensionality of comparison and allow for a comparison between conditions with a single number as the figure of merit. This comparison in staining quality is only appropriate when the target antigen is consistently distributed throughout the tissue, which may not always be the case.

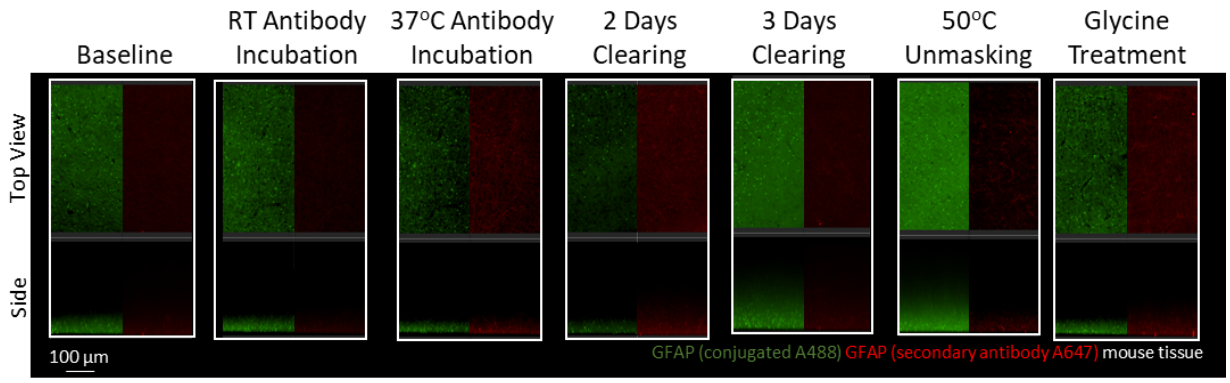

Figure S10. Immunohistochemistry with GFAP antibodies in with PFA-hydrogelled mouse brain tissue. Representative maximum intensity projection views from the top and side of 500µm thick, 5mm wide tissue sections of C57Bl/6J mouse isocortex stained with two different antibodies for GFAP. Monoclonal GA5 conjugated to Alexa Fluor 488 (green) was stained and imaged in the same tissue as a polyclonal antibody using a goat anti-rabbit secondary conjugated to Alexa Fluor 647 (red).

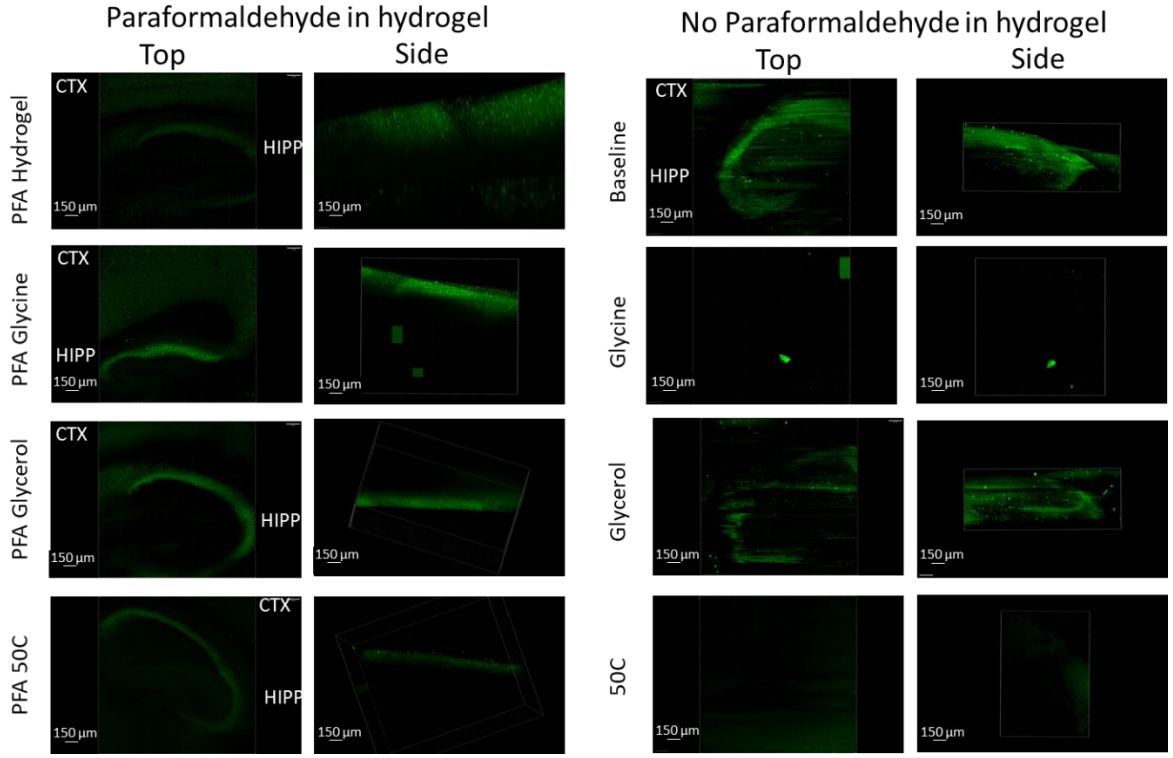

Figure S11. Immunohistochemistry of dopamine receptor 2 in mouse brain tissue. Representative maximum intensity projection views from the top and side of 1mm thick sagittal slices of C57Bl/6J mouse brain. Dopamine receptor 2 (green) shows significantly better fluorescent labeling in both the cortex (CTX) and hippocampus (HIPP) when the tissue is prepared with PFA in hydrogel.

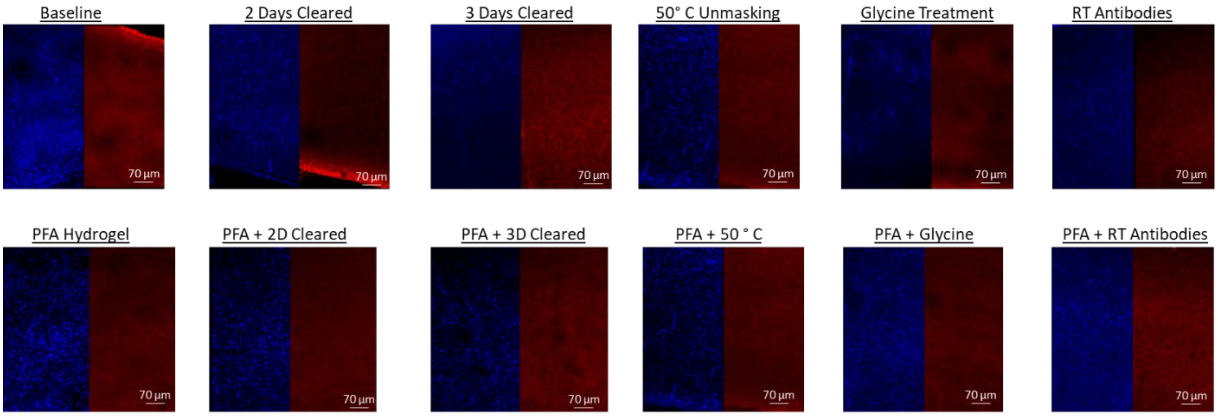

Figure S12 AT8 and HT7 immunohistochemistry in mouse tissue expressing human tau (Htau). Representative maximum intensity projection views from the top of 500µm thick, 5mm wide tissue sections of HTau mouse isocortex AT8 (Blue) and HT7 (Red) show labeling of tau in mice expressing human tau in the same conditions that show staining in human tissue.

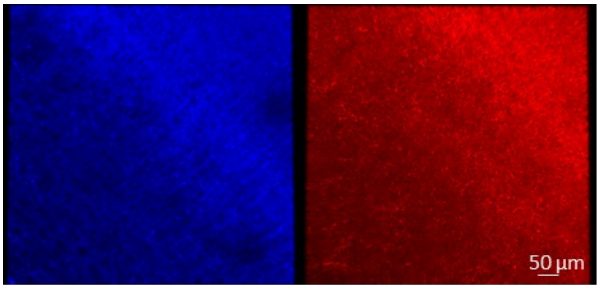

Figure S13 AT8 and HT7 immunohistochemistry in tau knockout mice (Htau KO). Representative maximum intensity projection views from the top of 500µm thick, 5mm wide tissue sections of Htau knockout mouse isocortex. AT8 (Blue) and HT7 (Red) show no labeling of tau in knockout mice using the same baseline conditions where they show labeling in Htau mice expressing human tau.

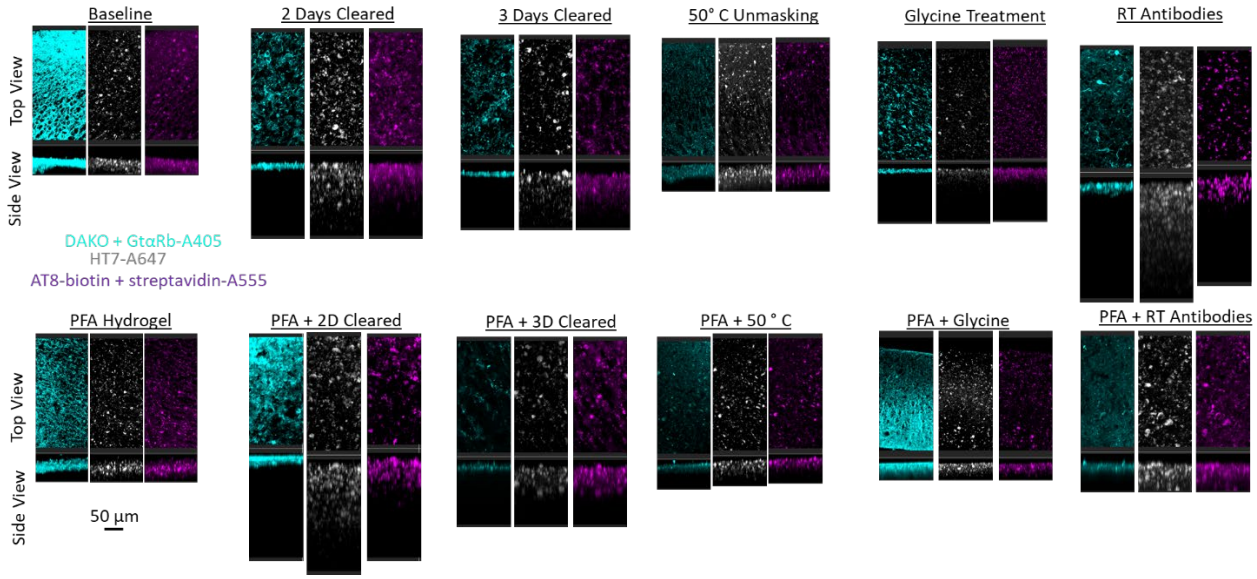

Figure S14 Additional Dako, AT8, and HT7 Tau immunohistochemistry conditions in human brain tissue Representative maximum intensity projection views from the top and side of 500µm thick, 5mm wide tissue sections from frozen human tissue samples.

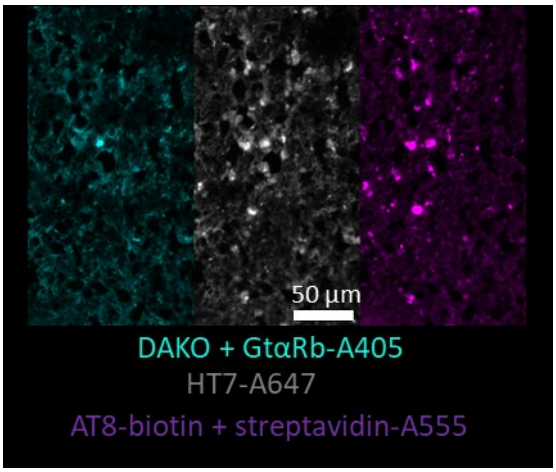

Figure S15 Representative microtome images taken from the human tissue prior to clearing. Human tissue was stained with Dako, AT8, and HT7 to confirm the presence of their target Tau prior to testing large volume IHC conditions.

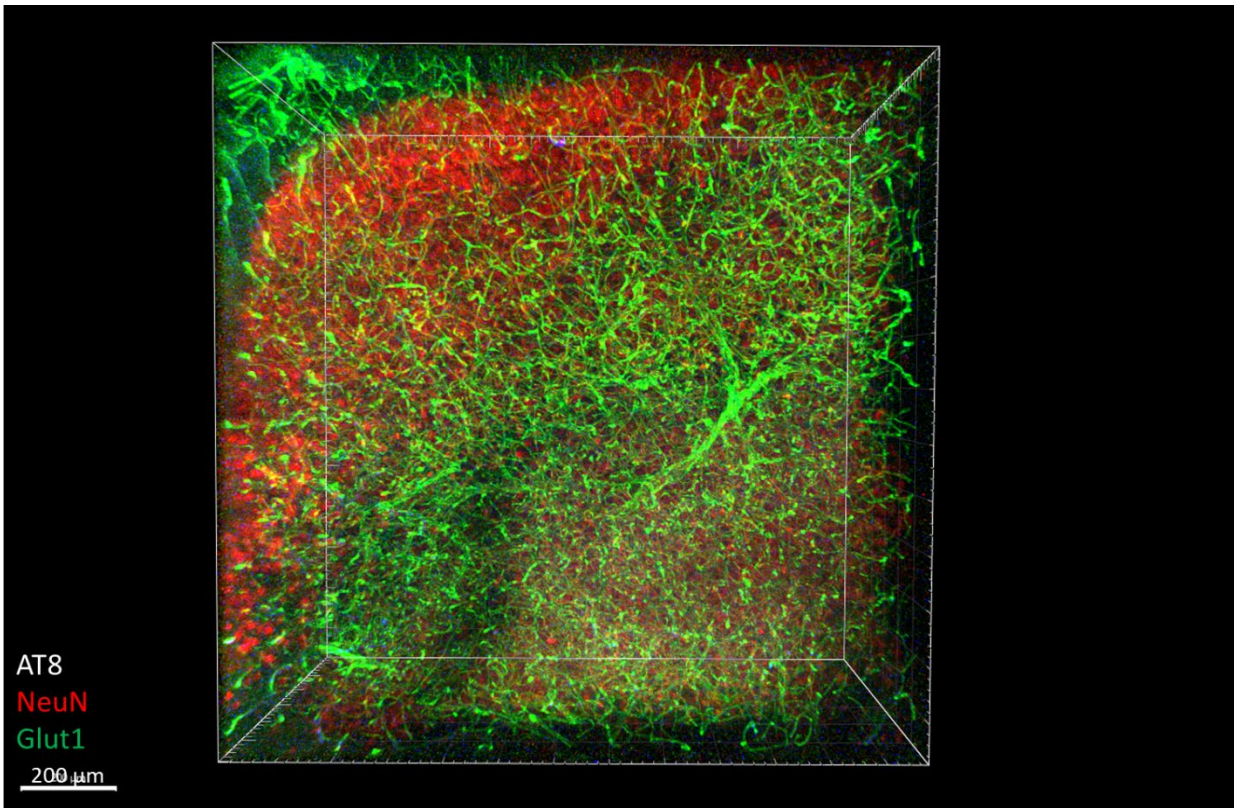

Figure S16 Immunohistochemistry in 1mm mouse tissue The tissue was crosslinked without PFA, cleared for 2 days, rinsed, then the antibodies NeuN-A568 (Red), Glut1-A488 (Green), and AT8-A647 (Blue) were incubated with the tissue for 14 days. A small section of the total stained tissue was imaged and shows complete staining throughout the entire thickness of the sample.

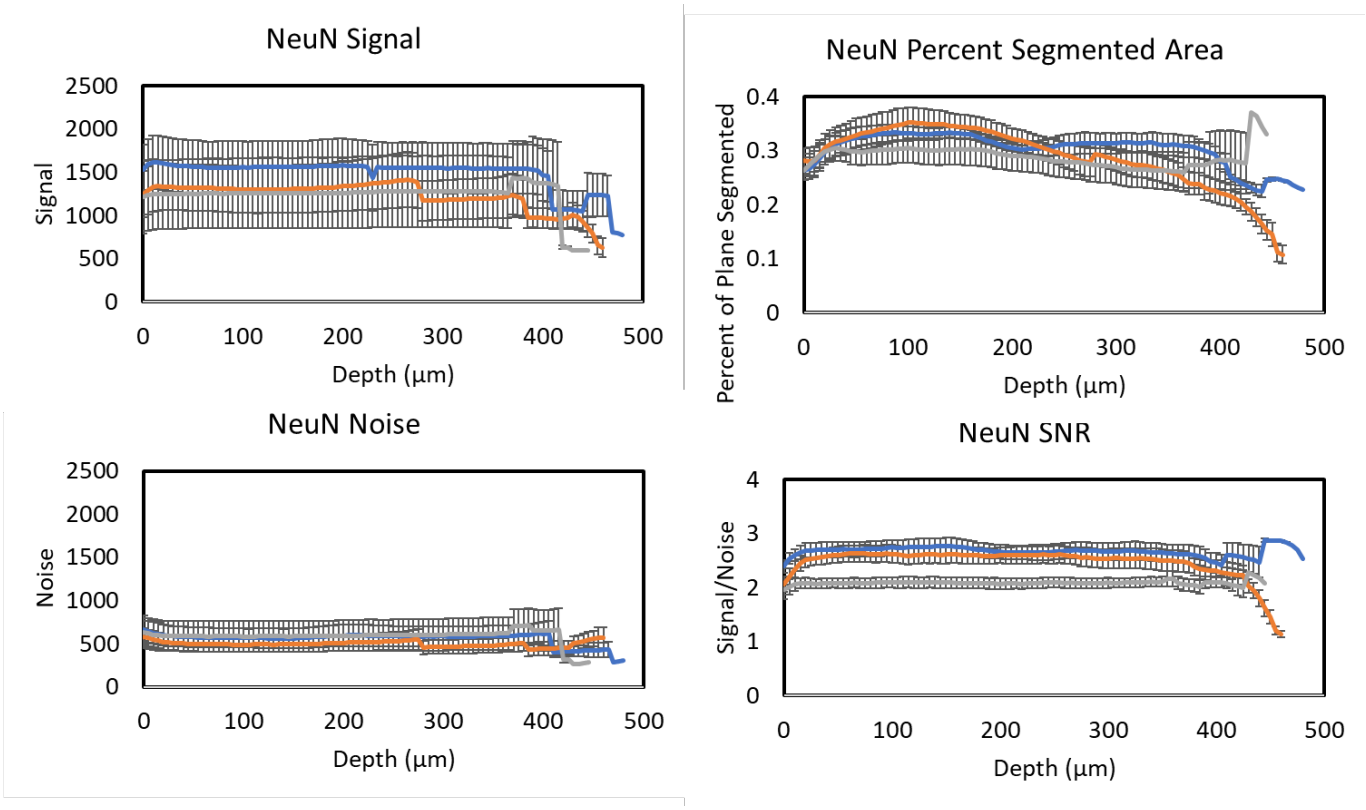

Figure S17. Immhunohistochemistry staining consistency across brain regions. Average signal intensity of immunohistochemistry labeling with NeuN-A568 in ~500µm thick mouse cortex tissue prepared using optimized conditions and incubated with antibodies for 3 days. n = 6 independently prepared longitudinal sections from 3 different mice. Each section was imaged at the hippocampus (blue), posterior cortex (grey), and anterior cortex (orange).

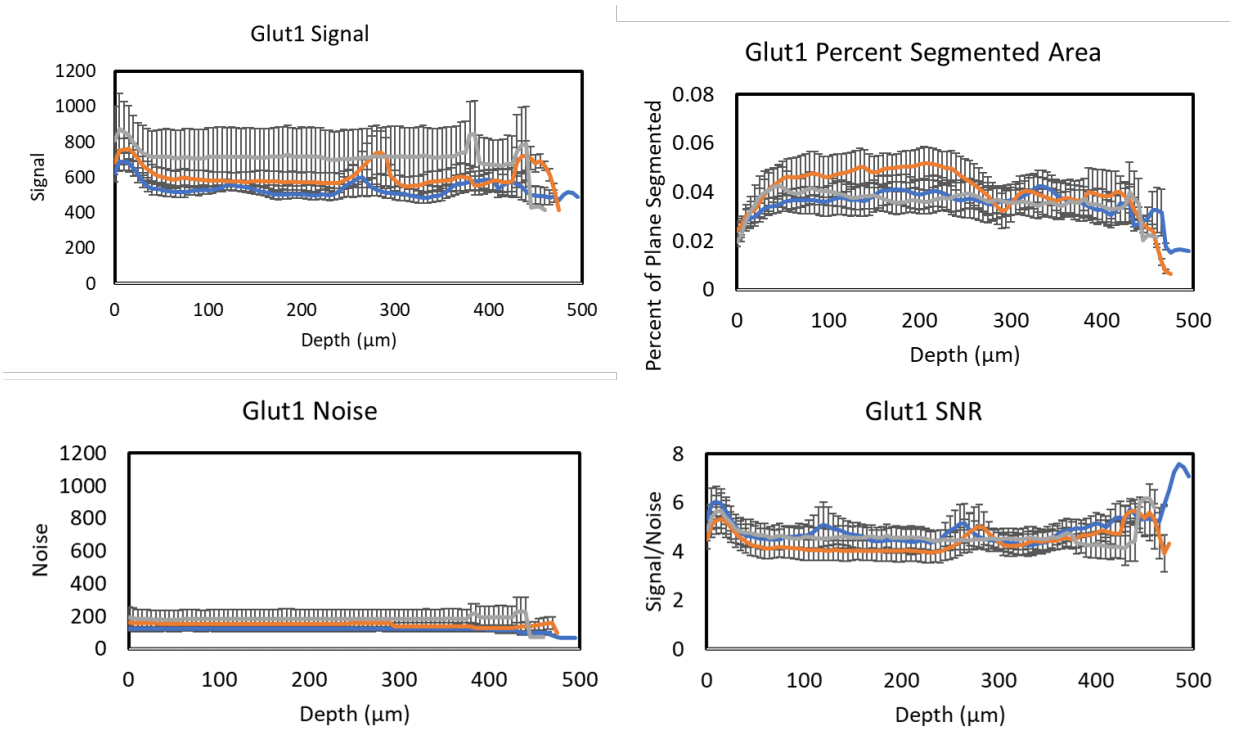

Figure S18. Immhunohistochemistry staining consistency across brain regions. Average signal intensity of immunohistochemistry labeling with Glut1-A488 in ~500µm thick mouse cortex tissue prepared using optimized conditions and incubated with antibodies for 3 days. n = 6 independently prepared longitudinal sections from 3 different mice. Each section was imaged at the hippocampus (blue), posterior cortex (grey), and anterior cortex (orange).

Sample Number	Sex	Age at Death	Braak Staging	Hemisphere	Comorbidities
1 (1581)	M	89	VI	Frozen Left	CVD and CAA
2 (1762)	F	71	VI	Frozen Right	CVD and CAA
3 (2620)	M	52	N/A	Frozen Right	N/A

Supplementary table 1. Demographic and characteristics of all subjects used in this study including sex (M = Male ; F = Female), Age at death, Braak stage, Hemisphere, CerebroVascular Disease (CVD), and Cerebral Amyloid Angiopathy (CAA).